

AD-A060 203

CINCINNATI UNIV OH DEPT OF AEROSPACE ENGINEERING AND--ETC F/G 20/4
NUMERICAL SOLUTIONS OF THE TRIPLE-DECK EQUATIONS FOR SUPERSONIC--ETC(U)
JUN 78 M NAPOLITANO, M J WERLE, R T DAVIS

N00014-76-C-0359

UNCLASSIFIED

AFL-78-6-42

NL

1 OF 2
AD
A0 60203



12 LEVEL II

AD A060203



NUMERICAL SOLUTIONS OF THE TRIPLE-DECK EQUATIONS
FOR SUPERSONIC AND SUBSONIC FLOW PAST A HUMP

M. NAPOLITANO, M.J. WERLE
AND R.T. DAVIS

[Handwritten signature]

DDC FILE COPY

Approved for public release; distribution unlimited.

This research was supported by the Naval Sea Systems
Command General Hydromechanics Research Program
administered by the David W. Taylor Naval Ship Research
and Development Center under Contract N00014-76-C-0359.

June 1978



78 10 10 081

NUMERICAL SOLUTIONS OF THE TRIPLE-DECK EQUATIONS
FOR SUPERSONIC AND SUBSONIC FLOW PAST A HUMP

M. Napolitano*, M.J. Werle** and R.T. Davis***

Aerospace Engineering and Applied Mechanics Department
University of Cincinnati
Cincinnati, Ohio

This research was supported by the Naval Sea Systems
Command General Hydromechanics Research Program
administered by the David W. Taylor Naval Ship Research
and Development Center under Contract N00014-76-C-0359.

Distribution of this report is unlimited.

* Research Associate; also Assistant Professor at the
University of Bari, Italy.

** Formerly Professor; currently Chief, Gas Dynamics
Section, UTRC, East Hartford, Connecticut.

***Professor and Head.

78 10 10 081

NUMERICAL SOLUTIONS OF THE TRIPLE-DECK EQUATIONS
FOR SUPERSONIC AND SUBSONIC FLOW PAST A HUMP

M. Napolitano, M.J. Werle and R.T. Davis

ABSTRACT

An efficient Alternating Direction Implicit numerical technique is developed for solving the Triple-Deck fundamental problem for supersonic and subsonic flow. Flow past a hump on a flat plate is considered as a test case. Accuracy and reliability of the method are positively tested versus linearized equation results for a small hump height. Full nonlinear flow patterns are feasible, including mild separation. Numerical difficulties are encountered around the reattachment point for large hump heights.

ACCESSION FOR	
NTIS	White Section <input checked="" type="checkbox"/>
DDC	Buff Section <input type="checkbox"/>
UNANNOUNCED	<input type="checkbox"/>
JUSTIFICATION	
BY	
DISTRIBUTION/AVAILABILITY CODES	
Dist. ANAL. and/or SERIAL	
A	

TABLE OF CONTENTS

	<u>Page</u>
I INTRODUCTION	1
II THE FUNDAMENTAL TRIPLE-DECK PROBLEM	6
1. Governing Equations	6
2. Mathematical Character of the Equations . .	9
3. Prandtl Transposition Theorem	11
4. Jump Conditions for Supersonic Flow	13
III NUMERICAL METHOD FOR SUPERSONIC FLOW	16
1. The ADI Relaxation Technique	16
2. * Sweep Finite Difference Equations and Superposition Technique	18
3. Solution of the n+1 Time Sweep Equation . .	23
4. Windward Differencing and Jump Conditions. .	30
IV NUMERICAL METHOD FOR SUBSONIC FLOW	33
1. Second Sweep Equation	33
2. * Sweep Slope Discontinuities Treatment. . .	38
3. n+1 Sweep Slope Discontinuities Treatment	39
4. Alternate Approach for the n+1 Time Sweep Solution	41
V RESULTS	45
1. Supersonic Flow Results	45
2. Subsonic Flow Results	49
VI REFERENCES	56
APPENDIX A - INVERSION PROCEDURE FOR THE * SWEEP FINITE DIFFERENCE EQUATIONS	59

	<u>Page</u>
APPENDIX B - NUMERICAL SOLUTION OF CAUCHY INTEGRALS	63
APPENDIX C - A VECTORIZATION OF LOGARITHMS IN THE CAUCHY INTEGRAL SOLVER	69
APPENDIX D - ANALYTICAL EVALUATION OF FAR FIELD ASYMPTOTIC CONTRIBUTION TO THE CAUCHY INTEGRALS	72
APPENDIX E - CAUCHY INTEGRAL OF A DISCONTINUOUS FUNCTION	75

LIST OF FIGURES

<u>Figure</u>	<u>Page</u>
1a. Triple-Deck Structure Around a Small Hump	78
1b. Parabolic Hump in Bottom Deck Scaling	78
1c. Quartic Hump in Bottom Deck Scaling	78
2. Supersonic Flow Past a Parabolic Hump; Normalized Wall Shear and Pressure Profiles for $h = 0.1$. .	79
3. Supersonic Flow Past a Parabolic Hump; Longi- tudinal Step Size Study	80
4. Supersonic Flow Past a Parabolic Hump; Normal Step Size Study	81
5. Supersonic Flow Past a Parabolic Hump; Normalized Wall Shear Dependence on h	82
6. Supersonic Flow Past a Parabolic Hump; Normalized Pressure Dependence on h	83
7. Supersonic Flow Past a Parabolic Hump; Normalized Displacement Thickness Dependence on h	84
8. Supersonic Flow Past a Parabolic Hump; Normalized Longitudinal Velocity Dependence on h	85
9. Supersonic Flow Past a Parabolic Hump; Wall Shear Dependence on h	86
10. Subsonic Flow Past a Parabolic Hump; Normalized Wall Shear Profile for $h = 0.1$	87
11. Subsonic Flow Past a Parabolic Hump; Normalized Pressure Profile for $h = 0.1$	88
12. Subsonic Flow Past a Parabolic Hump; Longitudinal Step Size Study for Wall Shear	89
13. Subsonic Flow Past a Parabolic Hump; Longitudinal Step Size Study for Pressure	90
14. Subsonic Flow Past a Parabolic Hump; Normalized Wall Shear Dependence on h	91
15. Subsonic Flow Past a Parabolic Hump; Normalized Pressure Dependence on h	92

<u>Figure</u>	<u>Page</u>
16. Subsonic Flow Past a Quartic Hump; Longitudinal Step Size Study for Wall Shear	93
17. Subsonic Flow Past a Quartic Hump; Longitudinal Step Size Study for Pressure	94
18. Subsonic Flow Past a Quartic Hump; Longitudinal Step Size Study for Pressure	95
19. Subsonic Flow Past a Quartic Hump; Normalized Wall Shear and Pressure Profiles for $h = 0.1$. .	96
20. Subsonic Flow Past a Quartic Hump; Wall Shear Profile for $h = 3$	97
21. Subsonic Flow Past a Quartic Hump; Pressure Profile for $h = 3$	98
22. Cauchy Integral Model Problem Step Size Study . .	99
23. Cauchy Integral Model Problem Step Size Study . .	100
24. Cauchy Integral Model Problem Step Size Study . .	101

LIST OF SYMBOLS

AL	logarithms in the Cauchy Integrals evaluation
a,b	limits of integration for Cauchy Integrals
A,B,C,H _i ,	coefficients of the tridiagonal matrix, Eq. (3.25)
A _j ,B _j ,C _j ,H _j a _{5j} ,c _j ,d _j	coefficients of the finite difference equations (A1) and (A2)
CI	Cauchy Integral
d,∂	differentiation signs
D	total displacement, given in Eq. (2.7)
E _i ,F̄ _i	recursion coefficients in Thomas Algorithm, Eq. (3.26)
E _j ,F̄ _j ,G _j	recursion coefficients in Davis coupled scheme, Eq. (A3)
f	arbitrary function, argument of Cauchy Integrals
F(x)	normalized hump profile
h	hump height parameter
H.O.T.	Higher Order Terms
I(x)	far field integrals (Appendix D)
k	constant used in Eqs. (3.34) and (D3)
L	characteristic geometry length
O	of the order of
p	nondimensional Triple-Deck pressure
Re	Reynolds number, $Re = U_r L/\nu$
R,S	constant values for the argument of the Cauchy Integral (Appendix E)
t	nondimensional time
u	nondimensional lower deck longitudinal velocity component

U, \tilde{u}	longitudinal velocity components given in Eq. (3.7)
v	nondimensional lower deck normal velocity component
U_r	reference free-stream velocity
x^*	physical longitudinal coordinate
x	lower deck nondimensional longitudinal coordinate
\tilde{x}	transposed x coordinate
\bar{x}	shifted x coordinate ($\bar{x} = x + \Delta x/2$)
y^*	physical normal coordinate
y	lower deck nondimensional normal coordinate
w	transposed lower deck nondimensional normal velocity component
W, \tilde{w}	normal velocity components given in Eq. (3.8)
z	transposed lower deck nondimensional normal coordinate
γ	exponent for downstream algebraic decay of δ used in Eq. (3.34)
Δ	step size
δ	viscous displacement thickness
ϵ	Triple-Deck small perturbation parameter, $\epsilon = Re^{-1/8}$
$\bar{\epsilon}$	arbitrary small quantity
η	dummy variable of integration used in Appendix D
θ	Lighthill's constant, $\theta = 0.8272$
λ	twice the inverse of the time step, $\lambda = 2/\Delta t$
ν	kinematic viscosity
ξ	dummy variable of integration in the Cauchy integrals

τ	nondimensional shear, $\tau = \frac{\partial u}{\partial z}$
τ_w	nondimensional wall shear, $\tau_w = \left(\frac{\partial u}{\partial z}\right)_{z=0}$
x	outer edge boundary condition for the shear in the superposition technique

Subscripts

$i-1, i, i+1,$ $1, 2, 3,$ $j-1, j, j+1,$ k, I, J	grid point location
p	previous iteration in $n+1$ time step inner loop
x, y, z	partial (or total, only for x) derivative with respect to the indicated variable
$- +$	immediately ahead of and behind the indicated location

Superscripts

'	differentiation
$n, *, n+1$	time level in the ADI scheme
o	previous time level value

I. INTRODUCTION

In recent years the problem of high Reynolds number laminar separation has received a systematic analysis through the asymptotic Triple-Deck theory of Stewartson, Sychev, Neiland and Messiter (Refs. 1-7). Stewartson (Ref. 3), in particular, has shown that in many cases of practical interest, for sufficiently small separation causing disturbances, the structure of the separation region can be analytically represented by a three layer model which he named the "Triple-Deck". Three regions are identified, all having a characteristic longitudinal length of order $\epsilon^3 L$; L is the characteristic length of the geometry (usually the flat plate leading the disturbance region) and ϵ is the small parameter in the perturbation expansion, related to the large characteristic flow Reynolds number by the relation $\epsilon^8 = 1/Re$. The outer region (outer deck) is shown to have a characteristic length normal to the body surface also of order $\epsilon^3 L$ and is characterized by inviscid irrotational flow. The middle region (middle deck) has a normal characteristic length of order $\epsilon^4 L$ and is basically a displaced (Blasius) boundary layer flow, inviscid but rotational in nature, whose main effect is to passively communicate the pressure interaction between the outer and inner decks. This last region (lower deck) is

a viscous region of characteristic height of order $\varepsilon^5 L$, for which simplified boundary-layer-like equations hold and which is produced by the necessity for the flow field to accommodate the viscous boundary conditions at the body surface. (Figure 1a gives a sketch of the Triple-Deck structure.)

After nondimensionalization of the governing equations, the entire flow field around the separation region is determined to first order in the small perturbation parameter ε , by solving the fundamental Triple-Deck problem. This consists of the bottom deck boundary-layer-like equations coupled to a pressure interaction law, relating the viscous displacement thickness growth and the inviscid outer deck pressure gradient, according to linear airfoil theory.

Solutions to the Triple-Deck equations are important for two reasons: first they provide rational, complete solutions for high Reynolds number flows where the classical boundary layer approach fails (e.g. in regions where separation and reattachment occur); second, they are a reliable test base for assessing more comprehensive flow equation solvers (e.g. numerical algorithms for the Navier Stokes or Interacting Boundary Layer equations; Ref. 10).

Analytical solutions for the Triple-Deck problem can only be obtained for the linearized version of these equations, that apply when the perturbation producing geometry is small

in the bottom deck scaling (see Refs. 8 and 9 for example). Solution of the general problem can only be done numerically due not only to the nonlinear nature of the equations, but also to the fact that the pressure interaction law makes them of the boundary value type in the longitudinal direction. (This is true even for the case of supersonic Triple-Deck flow.)

To date, only a limited number of such solutions have been obtained for this general equation set. Solutions are available, for example, for the free interaction phenomenon between a shock wave and a boundary layer flow (Refs. 2, 12), for supersonic flow past compression and expansion corners (Refs. 13-15) and forward and backward facing steps (Ref. 15). Subsonic flow at the trailing edge of a finite flat plate has also been studied by several investigators independently (Refs. 7, 16 and 17). For this case it has been found that some of the results of this $Re \rightarrow \infty$ asymptotic theory are surprisingly accurate for moderate and even low values of the Reynolds number and are of great practical importance for calculating the viscous drag on a finite flat plate or on a thin airfoil with a sharp trailing edge (see Ref. 17 for example). Finally, it has been postulated that the Triple-Deck equations are valid around the separation point even in the case of catastrophic separation as in the flow past a circular cylinder (Refs. 4, 18). It has just recently been found that numerical solutions of this set of

equations are indeed possible in the circular cylinder case and confirm the postulated structure of the separation phenomenon (Ref. 19).

While definite advances are being made in the understanding of interaction flows through use of the Triple-Deck concept, progress is being slowed by the general inefficiency of most solution techniques available for this problem in the literature. Due to the boundary value and highly nonlinear nature of the problem, they are usually iterative procedures with two or more nested iteration loops, which require a large amount of computational effort (see Ref. 16 for example). For the subsonic case, in particular, numerical convergence is extremely slow and delicate: severe underrelaxation is required and in some cases an initialization reasonably close to the sought after solution is necessary to avoid divergent behavior. Here the Alternating Direction Implicit (ADI) relaxation technique successfully applied in many "elliptic" two dimensional flow problems (see Refs. 10 or 11 for example) is taken into consideration. The ADI approach developed by Werle and Vatsa (Ref. 20), for solving the supersonic Interacting Boundary Layer equations, is generalized here to provide an efficient Triple-Deck solver for both supersonic and subsonic flows. Results have been obtained for three flow configurations: supersonic and subsonic flow past a parabolic hump (Fig. 1b), and subsonic flow past a

quartic hump (Fig. 1c). Comparisons have been made in all cases with available solutions (numerical nonlinear or analytical linear) to assess the reliability and efficiency of the solution method. Wall shear and pressure distribution profiles are presented for a wide range of flow conditions, including separation.

II. THE FUNDAMENTAL TRIPLE-DECK PROBLEM

1. Governing Equations

The present work is primarily concerned with the numerical solution of the fundamental Triple-Deck equations for supersonic as well as subsonic flow conditions. Therefore, whereas such a set of equations will be discussed here in detail, only a very brief outline of the theoretical work which led to the formulation of the Triple-Deck theory will be presented. For the reader interested in more details, Stewartson (Ref. 3) provides a review of all the theoretical advances and results of interest related to "Multi-structured Boundary Layers on Flat Plates and Related Bodies" up to 1974. This article is the most complete description to date of the asymptotic Triple-Deck laminar separation theory, whose formulation is due to Stewartson himself more than to anyone else. Also of interest is Jenson's historical outline (Ref. 15) of the scientific struggle that led from the basic understanding of the interaction between a shock wave and a boundary layer to the formulation of a fully consistent asymptotic theory for laminar (supersonic flow) separation. Reference (15) also reviews the practical problems to which such a theory is applicable.

In the present study a simple physical problem will be briefly discussed to provide a basic understanding of the

asymptotic Triple-Deck structure and of the Triple-Deck (fundamental problem) equations, which will then be given without derivation. Viscous flow over a flat plate is considered (see Figure 1a). The flat plate has, at a distance L from its leading edge, an excrescence or hump of characteristic length and height of order $\epsilon^3 L$ and $\epsilon^5 L$ respectively; ϵ^8 is the inverse of the characteristic Reynolds number, $\epsilon^8 = \nu/U_\infty L = 1/Re$, such that $\epsilon \ll 1$. Since the hump is "asymptotically" small in physical variables, it is reasonable to expect that at a large enough distance ahead of and behind the hump the flow field will recover the undisturbed Blasius boundary layer flow characteristic of a flat plate geometry. Near the hump, though, the disturbance can be large enough to cause flow separation and a fine scale analysis is required to determine the important physical parameters such as wall shear and heat transfer coefficients. Figure 1b shows the small hump in the bottom deck reference system in which both its length and height $hF(x)$ are of order one. It has been shown (Refs. 3, 8) by rigorous asymptotic analysis that to first order in ϵ the flow field around the disturbance region (in this particular case the hump) is described by the following set of differential equations:

Continuity

$$\frac{\partial u}{\partial x} + \frac{\partial v}{\partial y} = 0 \quad , \quad (2.1)$$

and Momentum

$$u \frac{\partial u}{\partial x} + v \frac{\partial u}{\partial y} = - \frac{dp}{dx} + \frac{\partial^2 u}{\partial y^2} , \quad (2.2)$$

with boundary conditions:

$$u(x, hF(x)) = v(x, hF(x)) = 0 \quad (2.3a, b)$$

and

$$u(x, y \rightarrow \infty) \rightarrow y - \delta - h F(x) , \quad (2.4)$$

where δ is the viscous displacement thickness. The present set of equations is formally identical to the classical boundary layer ones, except for boundary condition (2.4). The important difference is due to the fact that the pressure gradient is not an imposed known function of x but "interacts" with the total displacement height D according to linear airfoil theory. That is, for supersonic flow conditions we have:

$$\frac{d^2 D}{dx^2} = \frac{dp}{dx} , \quad (2.5)$$

whereas in case of subsonic flow:

$$\frac{d^2 D}{dx^2} = \frac{1}{\pi} \oint_{-\infty}^{\infty} \frac{p_{\xi}}{x-\xi} d\xi , \quad (2.6)$$

where

$$D = \delta + hF(x) \quad (2.7)$$

and the integral in equation (2.7) is a Cauchy principal value one. The problem described by equations (2.1) through

(2.6) is obviously not yet "closed". Equations (3.1) and (3.2) are a set of parabolic partial differential equations and need initial conditions, given as

$$u(x \rightarrow -\infty, y) \rightarrow y \quad (2.8)$$

corresponding to the uniform shear flow constituted by the "bottom deck" undisturbed Blasius boundary layer. Equation (2.5), or (2.6) equivalently, accounts for the boundary value nature of the problem and requires the following boundary conditions:

$$\delta(x \rightarrow -\infty) \rightarrow 0 \quad (2.9)$$

and

$$\delta(x \rightarrow \infty) \rightarrow 0, \quad (2.10)$$

which again indicate the decaying nature of the disturbance far ahead of and behind the flow disturbing hump.

2. Mathematical Character of the Equations

There has been controversy about the mathematical nature of the Triple-Deck fundamental problem, which only very recently has been generally acknowledged to be of boundary value nature. In the supersonic case, in particular, the interaction law equation (2.5) can just as well be given as

$$\frac{dD}{dx} = \int_{-\infty}^x p_x dx, \quad (2.11)$$

and a marching solution technique, requiring no downstream boundary condition, would appear perfectly legitimate.

And, in fact, the first numerical method, used to solve the free interaction fundamental Triple-Deck problem, was a marching procedure (Ref. 2). Its failure of determining a unique solution for the reverse flow region was already acknowledged by the authors themselves (Ref. 2) to be caused by the lack of the necessary accounting for upstream propagation. A later computational technique, applied to the same free interaction problem, was instead able to provide a unique reverse flow solution by prescribing the asymptotic velocity profile downstream and marching backward toward the separation point (Ref. 12). The Triple-Deck equations for subsonic flow around the trailing edge of a flat plate were also numerically solved by a marching procedure (Ref. 16), and downstream recovery of the Goldstein wake solution was considered sufficient to prove that the solution procedure was well posed. Later, Jenson, Burggraf and Rizzetta (Ref. 13) developed a numerical scheme for solving the Triple-Deck equations for the ramp induced supersonic laminar separation. They properly accounted for the boundary value nature of the mathematical problem and were capable of determining a unique solution for any value of the normalized wedge angle even in the presence of very large separation bubbles. Further, the very similar Interacting Boundary Layer equations were solved for supersonic flow past a compression corner (Ref. 20). There it was found that branching could

not be avoided and that the weak interaction solution could not be numerically recovered unless the boundary value nature of the problem was taken into account by specifying appropriate downstream boundary conditions (see Ref. 20). It is therefore very clear that any numerical procedure developed for efficiently solving the Triple-Deck equations must properly account for the boundary value nature of the problem at hand in order to avoid the divergent behavior due to inappropriate branching solutions.

3. Prandtl Transposition Theorem

A numerical solution of the Triple-Deck problem would encounter the difficulty of prescribing the wall boundary conditions (2.3) on the body surface $hF(x)$, which does not necessarily coincide with the grid points in the computational domain. It is well known, though, (Ref. 21) that the Prandtl transposition theorem allows one to transpose the longitudinal coordinate axis to the body surface for the case of the classical Boundary Layer equations, which are formally identical to equations (2.1) and (2.2). Also, Jenson, Burggraf and Rizzetta (Ref. 13), Rizzetta (Ref. 14), and Jenson (Ref. 15), have successfully applied this concept to a numerical solution of the Triple-Deck equations for supersonic flow past a compression ramp. Here, following Jenson's lead, a new set of independent variables is introduced as:

$$\tilde{x} = x \quad (2.13)$$

and

$$z = y - hF(x) , \quad (2.14)$$

and the normal velocity component is also redefined according to

$$w = v - u hF'(x) . \quad (2.15)$$

Applying chain rule differentiation to both the u and v variables as follows

$$\frac{\partial u}{\partial x} = \frac{\partial u}{\partial \tilde{x}} - \frac{\partial u}{\partial z} h F'(x) \quad (2.16)$$

$$\frac{\partial u}{\partial y} = \frac{\partial u}{\partial z} , \quad (2.17)$$

and

$$\frac{\partial v}{\partial y} = \frac{\partial v}{\partial z} = \frac{\partial w}{\partial z} + \frac{\partial u}{\partial z} h F'(x) \quad (2.18)$$

and substituting equations (2.13) through (2.18) into the continuity and momentum equations (2.1) and (2.2), it is easily seen that these equations remain unchanged. Their final form is given below together with their modified boundary conditions.

$$\frac{\partial u}{\partial \tilde{x}} + \frac{\partial w}{\partial z} = 0 , \quad (2.19)$$

$$u \frac{\partial u}{\partial \tilde{x}} + w \frac{\partial u}{\partial z} = - \frac{dp}{d\tilde{x}} + \frac{\partial^2 u}{\partial z^2} , \quad (2.20)$$

$$u(\tilde{x}, 0) = w(\tilde{x}, 0) = 0 , \quad (2.21)$$

and

$$u(\tilde{x}, z \rightarrow \infty) \rightarrow z - \delta . \quad (2.22)$$

The interaction laws, equations (2.5) and (2.6), remain identically the same and are also given here for completeness as

$$\frac{d^2 D}{d\tilde{x}^2} = \frac{dp}{d\tilde{x}} \quad (2.23)$$

and

$$\frac{d^2 D}{d\tilde{x}^2} = \frac{1}{\pi} \oint_{-\infty}^{\infty} \frac{p_{\xi}}{\tilde{x} - \xi} d\xi \quad (2.24)$$

4. Jump Conditions for Supersonic Flow

In the case where the body surface under consideration, $hF(x)$, has one or more slope discontinuities, according to the theory of characteristics, it is possible that the flow variables also possess discontinuous derivatives at the corresponding points. Moreover, even if the flow variables, u, v and their derivatives (for example, $\partial u / \partial x$) were continuous across the points of discontinuity for $F'(x)$, the use of the Prandtl transposition theorem would induce discontinuous behavior in the normal velocity component w and the derivative of the longitudinal velocity component $\partial u / \partial \tilde{x}$. In fact, assuming that the point of discontinuity in $F'(x)$ is at the origin $x = 0$, that is

$$F'(0_+) \neq F'(0_-) \quad (2.25)$$

and assuming that v and $\partial u / \partial x$ are continuous across $x = 0$, equations (2.15) and (2.16), written immediately at the left (0_-) and at the right (0_+) of the origin, directly

provide the following jump conditions for w and $\partial u / \partial \tilde{x}$:

$$w(0_+) + uhF'(0_+) = w(0_-) + uhF'(0_-) \quad (2.26)$$

and

$$\frac{\partial u}{\partial \tilde{x}}(0_+) - \frac{\partial u}{\partial \tilde{z}} hF'(0_+) = \frac{\partial u}{\partial \tilde{x}}(0_-) - \frac{\partial u}{\partial \tilde{z}} hF'(0_-) . \quad (2.27)$$

It is therefore clear that a numerical algorithm, which solves the Triple-Deck equations for flow past a body with points of slope discontinuity and also makes use of the Prandtl transposition theorem, needs to properly account for the jump conditions given in equations (2.26) and (2.27).

In the case of supersonic flow past a sharp compression corner it can be proved that v and $\partial u / \partial x$ are indeed continuous through the corner point and, by simply assuming continuous pressure through the corner itself, the jump conditions (2.26) and (2.27) can be formally derived and the pressure gradient dp/dx can be proven to be continuous (Ref. 15). The same analysis applies as well to the case of supersonic flow past a hump with discontinuous slope at both the leading and trailing edges. In all these cases, higher derivatives are discontinuous even in the original x, y bottom deck variables and the corner points are origins of Goldstein sublayers, which eliminate these discontinuities. See Reference (15), which also gives a discussion of the structure of the Goldstein layer and its implications as to the accuracy of the numerical computations.

For subsonic flow past a hump with discontinuous slope (Ref. 8) as well as for the case of flow at the trailing edge of a flat plate (Ref. 16) (for which the discontinuity is in the "wall" boundary condition) $\partial u / \partial x$ as well as dp/dx and $d\delta/dx$ are not continuous at the points of discontinuity. It has instead been shown that in the bottom deck scaling $\partial u / \partial x \rightarrow \infty$ at the RHS (Right Hand Side) of the slope discontinuity point in the case of the hump (Ref. 8) and that dp/dx and $d\delta/dx \rightarrow \infty$ at the RHS of the trailing edge of the flat plate (Ref. 16). Of course these singularities are removed if a substructure of the bottom deck is considered and the Goldstein sublayer is properly accounted for. The present study makes no account of such a scaling. Therefore equations (2.26) and (2.27) will be properly accounted for, at any body slope discontinuity in the case of supersonic flow. For subsonic flow conditions, instead, a particular treatment will be needed for the points of discontinuity, to avoid improper differencing through them. The details will be given later in the section on numerical methods.

III. NUMERICAL METHOD FOR SUPERSONIC FLOW

1. The ADI Relaxation Technique

The numerical procedure, developed here for solving the fundamental Triple-Deck problem given in equations (2.19) through (2.24), is very similar to the one successfully applied by Werle and Vatsa (Ref. 20) to the solution of the supersonic interacting boundary layer equations in Levy Lees variables. A relaxation type time derivative for the total displacement D is added to the right hand side of the momentum equation (2.20) to give*:

$$uu_x + wu_z = -p_x + u_{zz} + \frac{\partial D}{\partial t} \quad (3.1)$$

and a two sweep relaxation technique proceeds in time from the n th step to $(n+1)$ th step in two increments of $\Delta t/2$. Over the first half time step (called the * step), the momentum equation (3.1) is written as

$$(uu_x + wu_z - u_{zz})^* = -p_x^n + \frac{2}{\Delta t} (D^* - D^n) \quad (3.2a)$$

whereas over the second half time step proceeding to t^{n+1} , it becomes

$$(uu_x + wu_z - u_{zz})^* = -p_x^{n+1} + \frac{2}{\Delta t} (D^{n+1} - D^*) \quad (3.2b)$$

* Note that equation (3.1) is not the unsteady bottom deck momentum equation which would contain the longitudinal velocity time derivative, $\partial u/\partial t$, and therefore only the "relaxed" solution will have physical meaning. Also, the \sim on the x coordinate is removed from now onward for convenience.

to give a formally second order accurate solution in Δt . Equation (3.2a) together with the continuity equation (2.19) constitutes a set of parabolic partial differential equations which is solved by a standard marching technique to provide the values of u^* , w^* , D^* , as later described in detail. (Note that at the $*$ time level the values p_x^n and D^n are known functions.) Proceeding to the $n+1$ time level by means of equation (3.2b), its left hand side will be known and the solution will provide the values for the total displacement, D^{n+1} , and the pressure gradient, p_x^{n+1} . Since these unknowns are directly related by the interaction law, equation (2.5), and are both independent of the normal coordinate, z , the second sweep equation (3.2b) is first simplified using equation (3.2a) to give

$$p_x^{n+1} - \lambda(D^{n+1} - D^*) = p_x^n - \lambda(D^* - D^n) , \quad (3.3)$$

where $\lambda = 2/\Delta t$ has been introduced for convenience. This, together with the interaction law, equation (2.5), finally gives:

$$D_{xx}^{n+1} - \lambda(D^{n+1} - D^*) = D_{xx}^n - \lambda(D^* - D^n) . \quad (3.4)$$

Note that the unknown second derivative, D_{xx}^{n+1} , is the term which properly allows for the boundary value nature of the Triple-Deck equations. The finite difference representation of equation (3.4) will later be seen to be able to directly accommodate the proper upstream as well as downstream boundary conditions on D^{n+1} .

2. Finite Difference * Sweep Equations and Superposition Technique

Figure I shows the computational grid used in the present numerical scheme. Indices $j-1$, j and $j+1$ are used to indicate the grid locations along the normal direction, z , whereas 1, 2 and 3 are used instead in the longitudinal x one. (Subscript i will also be used for the longitudinal direction.)

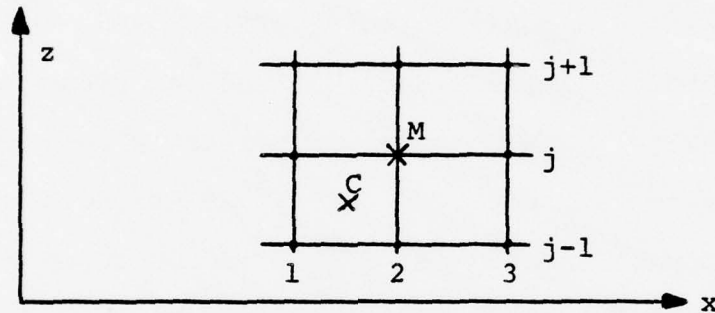


Figure I. Computational Grid

The finite difference equations for continuity and momentum are centered at points C and M respectively, and are given as follows:

Continuity

$$\frac{u_{2,j}^* - u_{1,j}^*}{\Delta x} + \frac{u_{2,j-1}^* - u_{1,j-1}^*}{\Delta x} + \frac{w_{2,j}^* - w_{2,j-1}^*}{\Delta z} + \frac{w_{1,j}^* - w_{1,j-1}^*}{\Delta z} = 0 \quad (3.5)$$

and Momentum

$$u_{1,j}^* \frac{(u_{2,j}^* - u_{1,j}^*)}{\Delta x} + \frac{1}{2} w_{1,j}^* \frac{u_{2,j+1}^* - u_{2,j-1}^*}{2\Delta z} + \frac{1}{2} w_{2,j}^* \frac{u_{1,j+1}^* - u_{1,j-1}^*}{2\Delta z} + (p_x^n)_2 - \lambda (D_2^* - D_2^n) - \frac{u_{2,j+1}^* - 2u_{2,j}^* + u_{2,j-1}^*}{\Delta z^2} = 0 \quad (3.6)$$

Note that the two convective terms in equation (3.6) have been linearized or quasilinearized around the previous station 1 and therefore equations (3.5) and (3.6) are both linear in their unknowns $u_{2,j}^*$ and $w_{2,j}^*$, which also linearly depend on the unknown total displacement D_2^* . A simple superposition technique can be used to solve the set of equations without iteration. Two new dependent variables are defined for each of the original ones, as follows:

$$u_{2,j}^* = U_j + D_2^* \tilde{u}_j \quad (3.7)$$

and

$$w_{2,j}^* = W_j + D_2^* \tilde{w}_j \quad (3.8)$$

and are then introduced in equation (3.5) and (3.6) to give:

$$\begin{aligned} & \frac{U_j + D_2^* \tilde{u}_j - u_{1,j}^*}{\Delta x} + \frac{U_{j-1} + D_2^* \tilde{u}_{j-1} - u_{1,j-1}^*}{\Delta x} + \frac{W_j + D_2^* \tilde{w}_j - w_{j-1} - D_2^* \tilde{w}_{j-1}}{\Delta z} \\ & + \frac{w_{1,j}^* - w_{1,j-1}^*}{\Delta z} = 0 \end{aligned} \quad (3.9)$$

and

$$\begin{aligned} & u_{1,j}^* \frac{U_j + D_2^* \tilde{u}_j - u_{1,j}^*}{\Delta x} + \frac{1}{2} w_{1,j}^* \left(\frac{U_{j+1} - U_{j-1}}{2\Delta z} + D_2^* \frac{\tilde{u}_{j+1} - \tilde{u}_{j-1}}{2\Delta z} \right) \\ & + \frac{1}{2} (W_j + D_2^* \tilde{w}_j) \frac{u_{1,j+1}^* - u_{1,j-1}^*}{2\Delta z} + (p_x^n)_2 - \lambda (D_2^* - D_2^n) \\ & - \frac{U_{j+1} - 2U_j + U_{j-1}}{\Delta z^2} - D_2^* \frac{\tilde{u}_{j+1} - 2\tilde{u}_j + \tilde{u}_{j-1}}{\Delta z^2} = 0 \end{aligned} \quad (3.10)$$

For equations (3.9) and (3.10) to be satisfied, it is necessary that all the coefficients of the total displacement D_2^* vanish, which condition produces the following set of equations for \tilde{u}_j, \tilde{w}_j :

$$\tilde{w}_j = \tilde{w}_{j-1} - \frac{\Delta z}{\Delta x} \tilde{u}_j - \frac{\Delta z}{\Delta x} \tilde{u}_{j-1} \quad (3.11)$$

and

$$\begin{aligned} & \left(\frac{1}{\Delta z^2} + \frac{w_{1,j}^*}{4\Delta z} \right) \tilde{u}_{j-1} - \left(\frac{2}{\Delta z^2} + \frac{u_{1,j}^*}{\Delta x} \right) \tilde{u}_j + \left(\frac{1}{\Delta z^2} - \frac{w_{1,j}^*}{4\Delta z} \right) \tilde{u}_{j+1} \\ & = -\lambda + \frac{1}{4\Delta z} (u_{1,j+1}^* - u_{1,j-1}^*) \tilde{w}_j . \end{aligned} \quad (3.12)$$

Consequently the remaining terms of equations (3.9) and (3.10) also vanish, that is:

$$w_j = w_{j-1} - \frac{\Delta z}{\Delta x} u_j - \frac{\Delta z}{\Delta x} u_{j-1} + \frac{\Delta z}{\Delta x} (u_{1,j}^* + u_{1,j-1}^*) - w_{1,j}^* + w_{1,j-1}^* \quad (3.13)$$

and

$$\begin{aligned} & \left(\frac{1}{\Delta z^2} + \frac{w_{1,j}^*}{4\Delta z} \right) u_{j-1} - \left(\frac{2}{\Delta z^2} + \frac{u_{1,j}^*}{\Delta x} \right) u_j + \left(\frac{1}{\Delta z^2} - \frac{w_{1,j}^*}{4\Delta z} \right) u_{j+1} \\ & = \lambda D_2^n + (p_x)_2^n - \frac{u_{1,j}^{*2}}{\Delta x} + \frac{1}{4\Delta z} (u_{1,j+1}^* - u_{1,j-1}^*) w_j . \end{aligned} \quad (3.14)$$

Equations (3.11) through (3.14) constitute two independent sets of difference equations for which appropriate boundary conditions can be easily obtained by splitting those for equations (3.9) and (3.10) by means of equations (3.7) and (3.8) as follows:

The wall no slip, zero injection conditions

$$u_{2,1}^* = w_{2,1}^* = 0 \quad (3.15a,b)$$

provide the following equations

$$U_1 = \tilde{u}_1 = W_1 = \tilde{w}_1 = 0, \quad (3.16a-d)$$

whereas the outer edge boundary condition*

$$\left(\frac{\partial}{\partial z} u_2^*\right)_J = 1 \quad (3.17)$$

gives

$$\left(\frac{\partial}{\partial z} U\right)_J = 1 \quad (3.18)$$

and

$$\left(\frac{\partial}{\partial z} \tilde{u}\right)_J = 0 \quad (3.19)$$

* Note that the outer edge boundary condition (2.4) is first imposed at a finite distance $z = z_{\text{edge}}$ ($j=J$) and then replaced by its derivative, in order to minimize the error produced by imposing an asymptotic boundary condition at a finite distance. The analytical linearized solution shows that the perturbation shear, $\partial u / \partial z$, decays at a slower rate than the velocity, u . Therefore, if the boundary condition is accurate enough for the shear, it will be definitely so for the velocity profile, but not vice versa. Also, the present superposition technique produced numerical boundary layers near the outer edge location for u_j and U_j when the velocity boundary condition was used. That is, the outer edge region was found to be one of extremely large gradients for \tilde{u}_j and U_j in order for them to satisfy the appropriate boundary conditions. Such behavior obviously produced large truncation errors. The use of a shear outer boundary condition was instead found to be fully satisfactory.

Equations (3.11) and (3.12) with their boundary conditions (3.16b,d) and (3.19) as well as equations (3.13) and (3.14), with boundary conditions (3.16a,c) and (3.18), can be numerically solved using the Davis coupled scheme (Ref. 22), thus providing the complete arrays U_j , W_j , \tilde{u}_j , \tilde{w}_j at the * time level. (Appendix A describes the details of the solution procedure.) In order to complete the star sweep of the present numerical procedure it remains to determine the value of the total displacement D_2^* . This can be done by using the velocity outer edge boundary condition (2.22) which by means of equation (3.7) can be written as

$$U_J + D_2^* \tilde{u}_J = z_J - (D_2^* - hF_2) . \quad (3.20)$$

Note that D_2^* is the only unknown in equation (3.20) and can immediately be solved for, to give

$$D_2^* = \frac{z_J - U_J + hF_2}{1 + \tilde{u}_J} . \quad (3.21)$$

Many alternate ways of evaluating D_2^* have been investigated. In particular the one obtained as described below has produced a higher convergence rate in some cases, probably because it explicitly accounts for the relaxation time derivative, $\partial D / \partial t$. The momentum equation is written at the outer edge in its finite difference form as

$$(z_J - \delta_1^*) \frac{\delta_2^* - \delta_1^*}{\Delta x} - \frac{1}{2} w_{1,J}^* - \frac{1}{2} w_{2,J}^* - (p_x^n)_2 + \lambda (\delta_2^* - \delta_2^n) = 0 . \quad (3.22)$$

The grouping $\frac{1}{2} (w_{1,J}^* + w_{2,J}^*)$ is then evaluated by integrating the continuity equation from $z = z_1$ to $z = z_J$ by the trapezoidal rule and the following final expression is obtained for $D_2^*(\delta_2^* + hF_2)$

$$D_2^* \left[\lambda + \frac{z_J - \delta_1^*}{\Delta x} + \sum_{j=2}^J \frac{u_j + u_{j-1}}{2\Delta x} \Delta z \right] = \lambda D_2^n + (p_x^n)_2 + (z_J - \delta_1^*) \frac{(\delta_1^* + hF_2)}{\Delta x} - \sum_{j=2}^J \frac{u_j + u_{j-1} - u_{1,j}^* - u_{1,j-1}^*}{2\Delta x} \Delta z . \quad (3.23)$$

It must be stressed that conditions (3.22) and (3.23) are fully consistent with each other and, after convergence, produce, as expected, identically the same results.

A somewhat similar superposition technique has been used by Sykes in his numerical solution of the Triple Deck fundamental problem for subsonic flow past a quartic hump (Ref. 23).

3. Solution of the $n+1$ Time Sweep Equation

The finite difference form of the second sweep equation (3.4) uses central differences to approximate the second derivatives D_{xx} and produces the following tridiagonal set of linear algebraic equations.

$$\begin{aligned} \frac{1}{\Delta x^2} D_{i-1}^{n+1} - \left(\frac{2}{\Delta x^2} + \lambda \right) D_i^{n+1} + \frac{1}{\Delta x^2} D_{i+1}^{n+1} \\ = \frac{D_{i-1}^n - 2D_i^n + D_{i+1}^n}{\Delta x^2} + \lambda (D_i^n - 2D_i^*) . \end{aligned} \quad (3.24)$$

Even though the direct inversion of equation (3.24) by the Thomas algorithm (Ref. 24) is a standard technique, it will be briefly outlined here to provide a more complete numerical treatment of the downstream boundary condition. Equation (3.24) is of the form

$$A D_{i-1}^{n+1} + B D_i^{n+1} + C D_{i+1}^{n+1} = H_i \quad (3.25)$$

and can be directly inverted by the simple recursion formula

$$D_i^{n+1} = E_i D_{i-1}^{n+1} + \bar{F}_i \quad (3.26)$$

where the coefficients E_i and \bar{F}_i are given respectively as

$$E_i = \frac{-A}{B + C E_{i+1}} \quad (3.27)$$

and

$$\bar{F}_i = \frac{H_i - C \bar{F}_{i+1}}{B + C E_{i+1}} \quad (3.28)$$

It is then clear that after the coefficients E_i and \bar{F}_i are determined at the last grid point, I , by means of the downstream boundary condition on D^{n+1} , all the coefficients E_i , \bar{F}_i can be evaluated through equations (3.27) and (3.28). Finally the recursion relation (3.26) gives the complete array of unknowns D_i^{n+1} once the initial boundary condition for D_1^{n+1} is provided. In the present study, the asymptotic upstream boundary condition $\delta(x \rightarrow -\infty) \rightarrow 0$ has been directly applied to D^{n+1} at a finite distance x_1 as

$$D_1^{n+1} = 0 \quad (3.29)$$

which was numerically proven to be a sufficiently good approximation. Several implementations of the asymptotic downstream boundary condition, $\delta(x \rightarrow \infty) \rightarrow 0$, were instead used in order to minimize the negative effect of the known slow algebraic decay for the displacement thickness δ . Here the case in which $F(x)$ is identically zero around the location x_I where the downstream boundary condition was imposed is considered in detail, the extension to the compression ramp geometry where $F(x) = x$ ($h = \bar{\alpha}$, Refs. 13-15) being straightforward.

The simplest way of imposing the downstream boundary condition is of course to impose at a finite, sufficiently large downstream location x_I

$$D_I^{n+1} = 0 \quad , \quad (3.30)$$

which is identically satisfied, for any step size Δx , by imposing

$$E_I = \bar{F}_I = 0 \quad . \quad (3.31a,b)$$

The simple observation that the derivative of an algebraically decaying function decays at a faster rate than the function itself, obviously suggests that the error of imposing an asymptotic boundary condition at a finite distance will be lower for a derivative condition, that is

$$\left(\frac{dD}{dx} \right)_I^{n+1} = 0 \quad . \quad (3.32)$$

Equation (3.32) can be easily seen to be numerically satisfied to first order accuracy by an analysis similar to that of Appendix A, but simpler, by setting

$$E_I = 1 \quad \text{and} \quad \bar{F}_I = 0 \quad . \quad (3.33a,b)$$

Usually the displacement thickness δ has an algebraic decay downstream, that is

$$D(x) \equiv \delta(x) \approx Kx^{-\gamma} \quad (\text{for } x \gg 1) \quad (3.34)$$

where γ is determined by asymptotic analysis whereas K can be left unknown for present purposes. Equation (3.34) differentiated once, provides the following relation between total displacement and its derivative

$$\frac{dD}{dx} \approx -\frac{\gamma}{x} D \quad (\text{for } x \gg 1) \quad . \quad (3.35)$$

The expression of dD/dx given by equation (3.35) is then used in a Taylor series expansion of $D^{n+1}(x)$ around the final grid point location x_I to give

$$D_{I-1} = D_I + \frac{\gamma \Delta x}{x_I} D_I + O(\Delta x^2) \quad (3.36)$$

which, written in the familiar form

$$D_I = \frac{1}{1 + \gamma \Delta x / x_I} D_{I-1} \quad (3.37)$$

finally provides the appropriate values for E_I , \bar{F}_I given respectively as

$$E_I = 1/(1 + \frac{\gamma \Delta x}{x_I}) \quad \text{and} \quad \bar{F}_I = 0 \quad . \quad (3.38a,b)$$

Note that more accurate implementation of this boundary condition could be straightforwardly obtained by using higher derivatives of $D(x)$ in the series expansion equation (3.36), if needed. Also note that this way of applying the downstream boundary condition at a finite distance x_I is of higher order accuracy in an asymptotic sense, with respect to both the previously discussed ones. This is because it properly accounts for the leading term in the analytical asymptotic expansion for $\delta(x)$, equation (3.34). The use of this boundary condition in the solution of the second sweep equation (3.4), though, provided very little advantage with respect to either equations (3.31) or (3.33). In fact, the numerical solution for D^{n+1} could not reach its analytical decay for values of x_I as large as 20, even though, a further increase of x_I caused the final solution to change only immediately before x_I itself. At the same time, the numerically evaluated coefficient E_i and \bar{F}_i were seen to take on constant values over a wide range of the independent variable x in the downstream region and then suddenly change to reach their imposed values at the last station x_I . This phenomenon seemed to indicate that the finite difference equation (3.24) possesses a somewhat different asymptotic behavior than the corresponding differential

equation. Allowing such a finite difference equation to take on its own asymptotic behavior, as described below, provided the most consistent and effective downstream boundary condition. Equations (3.27) and (3.28) are rewritten here for convenience

$$E_i = \frac{-A}{B + C E_{i+1}} \quad (3.27)$$

and

$$\bar{F}_i = \frac{H_i - C \bar{F}_{i+1}}{B + C E_{i+1}} \quad (3.28)$$

If E_i and \bar{F}_i must become constant for sufficiently large values of i , they must satisfy equations (3.27) and (3.28) with $E_{i+1} = E_i$ and $\bar{F}_{i+1} = \bar{F}_i$. Equation (3.27) thus becomes a quadratic algebraic equation for E_i , which, for the values of A , B and C given by Equation (3.24), gives the following two roots

$$E_i = 1 + \frac{\lambda \Delta x^2}{2} \pm \sqrt{\left(1 + \frac{\lambda \Delta x^2}{2}\right)^2 - 1} \quad (3.39)$$

The root corresponding to the minus sign is chosen in order to allow only for a decaying D_i^{n+1} . After, this expression (3.39) is substituted into (3.28) for E_i and the following "asymptotic" expression for \bar{F}_i is obtained

$$\bar{F}_i = \frac{2}{\lambda} \frac{-\frac{\lambda \Delta x^2}{2} H_i}{\frac{\lambda \Delta x^2}{2} + \sqrt{\left(1 + \frac{\lambda \Delta x^2}{2}\right)^2 - 1}} \quad (3.40)$$

Note that \bar{F}_i can become a constant for large x_i values only if the right hand side of equation (3.40), namely H_i , also becomes a constant. By analyzing the H_i expression

$$H_i = \frac{D_{i+1}^n - 2D_i^n + D_{i-1}^n}{\Delta x^2} + \lambda(D_i^n - 2D_i^*) \quad (3.41)$$

it is clear that for large values of x_i the second derivative of the total displacement D_{xx}^n as well as the displacement D_i^* and D_i^n should go to zero. Due to the truncation error of the numerical scheme instead, D_i was seen to become a finite constant downstream and H_i also took on a constant value for converged solutions. That is, for $D_i^{n+1} = D_i^* = D_i^n$, $H_i = \lambda D_i^*$, as clearly appears from equation (3.41). Using at the last grid point the values of E_I and \bar{F}_I , given by equations (3.39) and (3.40) respectively, was seen to eliminate the abrupt change in the solution in the neighborhood of the final station x_I . Enforcing the proper asymptotic decay of the finite difference equations also allowed the solution D_i to reach the same level of accuracy with smaller values of x_I . Finally, the numerical inaccuracy leading to constant downstream values for the total displacement D_i was seen to diminish by reducing the step size Δx , and these D_i values linearly vanished with Δx as they should.

4. Windward Differencing and Jump Conditions

It is well known that numerical techniques, using backward difference representations for the longitudinal convective term (uu_x in the present case) in viscous flow computations, face numerical instability in regions of reverse flow. This problem, which is basically due to the fact that no upstream information is accounted for, therefore violating the physics of the problem, is usually removed by windward differencing. The following finite difference form of the convective term uu_x in the momentum equation (3.6) at the * time level was therefore used in the present scheme

$$(uu_x)^* = \frac{u_1^* + |u_1^*|}{2} \frac{u_2^* - u_1^*}{\Delta x} + \frac{u_1^* - |u_1^*|}{2} \frac{u_3^{*0} - u_2^*}{\Delta x} . \quad (3.42)$$

Equation (3.42) automatically provides a backward representation for u_x if $u_1^* > 0$ and a forward one in case $u_1^* < 0$. In this case the value u_3^* must be taken from the previous time level u_3^{*0} . Also note that in equation (3.42) the j index has been dropped for simplicity and u_2^* stands for either U or \tilde{u} in the previously discussed superposition technique. No upwinding of the wu_z term was in general necessary as was the case for Jenson's numerical technique (Ref. 15).

For supersonic flow past a sharp compression corner or a parabolic hump, with slope discontinuities, the numerical procedure must be able to accommodate the

discontinuities or jumps in the w and $\partial u / \partial x$, due to the use of Prandtl transposition theorem.

In the previous chapter it was mentioned that the pressure gradient p_x and therefore D_{xx} (see equation 2.5) are continuous across the jump points. Therefore no special treatment is required in the second sweep equation and a central finite difference representation of D_{xx}^{n+1} is perfectly legitimate at every grid point. To properly treat the * sweep equations, the point of slope discontinuity must always coincide with a grid point in the computational mesh (see figure II)

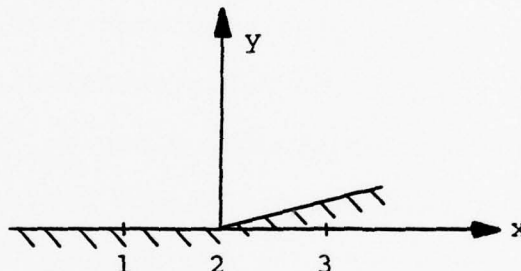


Figure II. Slope Discontinuity

In this way, while marching from point 1 to point 2 this point will be considered to lie immediately at the left of the slope discontinuity, ($2 \equiv 2_-$) and u_2^* and w_2^* can be determined in the usual manner. In marching from point 2 to 3, instead, point 2 must be considered to lie immediately at the right of the jump point ($2 \equiv 2_+$) in order for the finite difference representations, involving points 2 and 3, to have the expected order of accuracy.

This can be very easily obtained by simply updating the values of w_2^* by means of the known jump conditions equation (2.26) as soon as they have been evaluated. That is, after the step 1 to 2 has been completed, the w_2^* are adjusted to their proper values in order to proceed to the 2 to 3 step as follows

$$w_{2+}^* = w_{2-}^* - u_2^* h(F'_{2+} - F'_{2-}) \quad . \quad (3.43)$$

Equation (3.43) eliminates the need of storing the two different values of w_2^* and of selecting the appropriate one for each computation step; it is totally consistent with Jenson's jump condition treatment (Ref. 15) and was numerically found to be fully satisfactory. Note that with the present procedure, since $u_{2+} = u_{2-}$ and only forward or backward difference representations are used for u_x , any differencing through the jump is avoided; therefore, the discontinuous behavior for u_x is also properly accounted for.

IV. NUMERICAL METHOD FOR SUBSONIC FLOW

1. Second Sweep Equation

The only difference between the subsonic and supersonic Triple-Deck fundamental problem is the interaction law, equation (2.6). Accordingly, the numerical solution procedure for the subsonic case will be very similar to the supersonic one and only the major differences will be described here in detail. Equations (3.2a) and (3.2b) are valid in the subsonic case too and, by equating their right hand side, the following expression for p_x^{n+1} is first obtained

$$p_x^{n+1} = p_x^n + \lambda(D^{n+1} - 2D^* + D^n) , \quad (4.1)$$

which is identical to equation (3.3). Then, introducing the right hand side of equation (4.1) into the subsonic interaction law, equation (2.6), the final form of the second sweep equation is obtained as follows

$$D_{xx}^{n+1} = \frac{1}{\pi} \oint_{-\infty}^{\infty} \frac{p_{\xi}^n + \lambda(D^{n+1} - 2D^* + D^n)}{x - \xi} d\xi . \quad (4.2)$$

Note that equation (4.2) is the equivalent of equation (3.4) and this form is the one which properly allows for the boundary value nature of the problem.

The numerical solution of the * sweep difference equations proceeds exactly as in the supersonic case. (Very minor modifications necessary to account for the

unknown jump conditions will be indicated later.) The numerical solution of the second sweep equation (4.2) is instead very peculiar and will be discussed here in detail. The second derivative is first replaced by a central finite difference representation, and the Cauchy integral on the right hand side is broken into two parts to give:

$$\frac{D_{i+1}^{n+1} - 2D_i^{n+1} + D_{i-1}^{n+1}}{\Delta x^2} = \frac{1}{\pi} \oint_{-\infty}^{\infty} \frac{p_{\xi} d\xi}{x-\xi} + \frac{\lambda}{\pi} \oint_{\bar{x}_1}^{\bar{x}_{I-1}} \frac{D^{n+1} - 2D^* + D^n}{x_i - \xi} d\xi. \quad (4.3)$$

Note that $p_{\xi}(\xi)$ is a known function at all the grid points inside the numerical integration region $x_1 - x_I$. The major part of $\oint_{-\infty}^{\infty} \frac{p_{\xi} d\xi}{x-\xi}$ is $\oint_{\bar{x}_1}^{\bar{x}_{I-1}} \frac{p_{\xi} d\xi}{x-\xi}$ and is numerically evaluated by the methods described in Appendix B, whereas the residuals

$$\int_{-\infty}^{\bar{x}_1} \frac{p_{\xi} d\xi}{x-\xi} \quad \text{and} \quad \int_{\bar{x}_{I-1}}^{\infty} \frac{p_{\xi} d\xi}{x-\xi}$$

can be assessed if the asymptotic decay of $p(x)$ is known far ahead of and far behind the region of disturbance (see Appendix D for details). Also note that in equation (4.3) the Cauchy integral of the relaxation time dependent term has been approximated with its value over the region of numerical integration only*. This, because its purpose

* According to the Cauchy integral numerical evaluation given in Appendix A, a Cauchy integral can be evaluated either at a grid point x_i or at a midpoint $\bar{x}_i = \frac{x_i + \Delta x_i}{2}$. The corresponding regions of integration are $x_1 - x_{I-1}$ and $x_1 - x_I$ respectively.

is to allow the solution to relax to its steady state value and, after this has been reached, the integral vanishes. Unfortunately though, equation (4.3) cannot be reduced to a tridiagonal set of linear algebraic equations and inverted by Thomas Algorithm because of the presence of the unknown D^{n+1} inside the Cauchy integral. An iterative procedure is then necessary to solve the second sweep of the two step ADI method, equation (4.3). The most efficient solution procedure which we have been able to develop consists of extracting from the Cauchy integral the upper and lower diagonal entries for the D_i^{n+1} array, replacing all the others with their previous iteration level values $D_{p_j}^{n+1}$, and inverting the resulting tridiagonal matrix by the Thomas Algorithm. In more detail, the integral

$$CI(x_i) = \frac{\lambda}{\pi} \int_{x_1}^{\bar{x}_{I-1}} \frac{D^{n+1} - 2D^* + D^n}{x_i - \xi} d\xi \quad (4.4)$$

appearing in the right hand side of equation (4.3) is written in finite difference form according to equation (B2) of Appendix B at any location x_i and the tridiagonal elements contributions, namely $\frac{\lambda}{\pi} \ln 3 D_{i-1}^{n+1}$, 0, $-\frac{\lambda}{\pi} \ln 3 D_{i+1}^{n+1}$, are brought to the left hand side of equation (4.3). By also replacing all the other D_j^{n+1} contributors to the integral $CI(x_i)$ of equation (4.4) with their known previous iteration values $D_{p_j}^{n+1}$, equation (4.3) is reduced to the

following tridiagonal finite difference equation

$$\left(\frac{1}{\Delta x^2} - \frac{\lambda}{\pi} \ln 3\right) D_{i-1}^{n+1} - \frac{2}{\Delta x^2} D_i^{n+1} + \left(\frac{1}{\Delta x^2} + \frac{\lambda}{\pi} \ln 3\right) D_{i+1}^{n+1} = H_i \quad (4.5)$$

in which the known right hand side H_i also accounts for

the $\int_{x_1}^{\bar{x}_{I-1}} \frac{p_\xi^n d\xi}{x-\xi}$ contributor.

The inversion procedure for equation (4.5) is now identical to the one used for the second sweep equation (3.4) in the supersonic case, but it must be repeated until some convergence criterion for D_i^{n+1} and $D_{p_i}^{n+1}$ is met. As in many previous studies (Refs. 16 and 17), under-relaxation was found necessary to avoid divergent behavior. At the end of each iteration the new value of D_i^{n+1} obtained by inverting the tridiagonal matrix, equation (4.5), was underrelaxed according to the following relation

$$D_i^{n+1} \leftarrow 0.2 D_i^{n+1} + (1 - 0.2) D_{p_i}^{n+1} \quad (4.6)$$

in which the numerical value of the underrelaxation coefficient 0.2 was taken as in Ref. (16). Other under-relaxation coefficients were found to provide convergent behavior for the second sweep equation, but no systematic numerical study was made in order to find the optimal value. It was found that the relaxation parameter had to be lower than 0.5 in order to obtain convergent behavior.

Since the present relaxation technique does not provide a physically meaningful transient, a complete convergence in the second sweep iterative procedure was not necessary at every time step; a limit of 10 was therefore imposed for the number of iterations performed at each $n+1$ time level.

All the treatments of the boundary conditions described for the supersonic second sweep equation (3.4) apply as well to equation (4.5). Allowing the coefficients E_i , \bar{F}_i of the recursion formula, equation (3.26), to take on their "asymptotic" values was again found to be the most satisfactory approach. E_I and \bar{F}_I could then be determined exactly, as in the supersonic case of equations (3.39) and (3.40), to be

$$E_I = (1 - \frac{\lambda \ln 3}{\pi} \Delta x^2) / (1 + \frac{\lambda \ln 3}{\pi} \Delta x^2) \quad (4.7)$$

and

$$\bar{F}_i = \frac{H_I \Delta x^2}{E_I (1 + \frac{\lambda \ln 3}{\pi} \Delta x^2 - 2)} \quad (4.8)$$

\bar{F}_I was found to become practically zero in all converged numerical computations, but sometimes it grew without bound, thus inducing divergent behavior in the numerical procedure. Setting \bar{F}_I identically equal to zero (which it is to second order accuracy in Δx) was sufficient to remove this problem without deteriorating the accuracy of the solution.

2. * Sweep Slope Discontinuities Treatment

For subsonic flow past a parabolic hump with slope discontinuities, the linearized Triple-Deck equations (Ref. 8) produce pressure and wall shear distributions with discontinuous gradients at any point of slope discontinuity ($x = 0$), that is

$$\left(\frac{dp}{dx}\right)_{0+} \neq \left(\frac{dp}{dx}\right)_{0-}, \quad (4.9)$$

and

$$\left(\frac{\partial \tau_w}{\partial x}\right)_{0+} \neq \left(\frac{\partial \tau_w}{\partial x}\right)_{0-}, \quad (4.10)$$

where $\tau_w = \left(\frac{\partial u}{\partial z}\right)_{z=0}$. (4.11)

Furthermore, the wall shear gradient becomes singular at the right hand side of the slope discontinuity point (Ref. 8), that is

$$\left(\frac{\partial \tau_w}{\partial x}\right)_{0+} \rightarrow \infty. \quad (4.12)$$

It is obvious that, in the absence of analytically prescribed jump conditions, a special treatment of the finite difference equations is required to properly account for such behavior of the flow variables. The * sweep equations were treated as follows. The jump point was again made to always coincide with a grid point x_2 . In marching from point x_1 to x_2 , x_2 was considered to lie immediately ahead of the jump and the usual finite difference equations (3.5) and (3.6) were perfectly legitimate. In marching from point x_2 to x_3 ,

x_2 was considered to lie immediately at the right of the jump point and the following finite difference representations were used for the continuity equation and for the convective term wu_z in the momentum equation respectively.

$$\frac{1}{2} \frac{u_{3,j}^* - u_{2,j}^*}{\Delta x} + \frac{1}{2} \frac{u_{3,j-1}^* - u_{2,j-1}^*}{\Delta x} + \frac{w_{3,j}^* - w_{3,j-1}^*}{\Delta z} = 0 \quad (4.13)$$

and

$$w_{3,j}^* \frac{u_{2,j-1}^* - u_{2,j-1}^*}{2\Delta z} . \quad (4.14)$$

(Note that in equations (4.13) and (4.14) the unknown variables to which the superposition technique applies are $u_{3,j}^*$ and $w_{3,j}^*$.) The finite difference representations (4.13) and (4.14) eliminate the presence of the unknown $w_{2,j}^*$ array and avoids differencing across the jump point. They are therefore perfectly legitimate as long as $u_{2+}^* = u_{2-}^*$, that is the u-velocity is continuous across the jump, which it is. The modifications required for the coefficients of the inversion algorithm of Appendix A, in order to use equations (4.13) and (4.14) at each grid following a jump point are very straightforward.

3. n+1 Sweep Slope Discontinuities Treatment

It has been mentioned that the pressure gradient p_x is discontinuous across the points of slope discontinuity. The second derivative of the total displacement, given as

$$D_{xx} = \frac{1}{\pi} \oint_{-\infty}^{\infty} \frac{p_{\xi} d\xi}{x - \xi} \quad (2.6)$$

becomes singular in correspondence to the points of discontinuity for $\frac{dp}{dx}$. (See Appendix E for the analytical proof.) It appears therefore improper to express D_{xx} with a central difference at the corner points, since the Taylor series approach on which this representation is based evidently fails. In order to remove this problem the following approximation has been used to model dp/dx , which provides a correct evaluation of D_{xx} in the limit of zero step size and an "approximate" regular one for finite values of Δx .

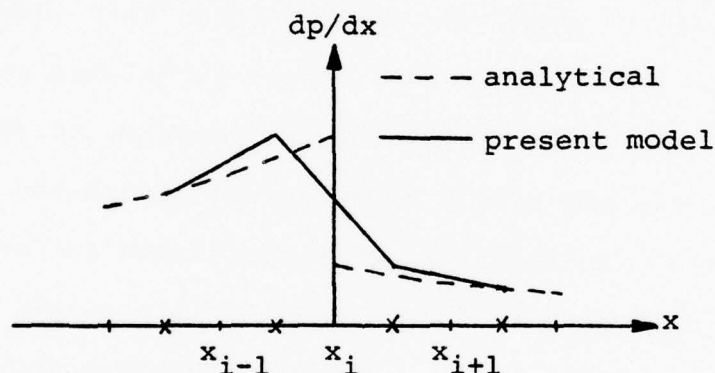


Figure III. Model for the Pressure Gradient Discontinuity.

Figure III shows an analytical function dp/dx discontinuous across x_i . In the present numerical procedure dp/dx is only known at each grid point x_i . However, in order to evaluate the Cauchy integral as described in Appendix B, dp/dx must be piecewise continuous across the midpoints \bar{x}_i . Therefore, dp/dx is taken as the average of the two neighboring grid point values at every \bar{x}_i but at those immediately before and after a jump point, where it is taken

equal to the successive grid point value. In this way the pressure gradient discontinuous jump is replaced by an equivalent (to first order) linear variation across one step size. Also, the corresponding value of $\oint_{x_1}^{x_I} \frac{dp/d\xi}{x-\xi}$ obtained by means of equation (B6) reproduces the same singular behavior obtained analytically for a discontinuous dp/dx for $\Delta x \rightarrow 0$ (see Appendix E for details). Moreover, it is regular for any finite Δx , thus allowing a central difference representation for D_{xx}^{n+1} . Numerical solutions obtained with such a model for the pressure gradient jump, show first order accurate behavior versus Δx at the jump points, thus confirming the validity of the present approach. However, an alternate more rational approach has also been used for further assessing the validity of the present numerical scheme.

4. Alternate Approach for the n+1 Time Step Solution

Most numerical schemes for solving the subsonic Triple-Deck equations (Refs. 16 and 17) use the following interaction law expression

$$D_x = \frac{1}{\pi} \oint_{-\infty}^{\infty} \frac{p(\xi)d\xi}{x-\xi} \quad (4.15)$$

This can be easily derived by the one given in equation (2.6)

$$D_{xx} = \frac{1}{\pi} \oint_{-\infty}^{\infty} \frac{p_{\xi}d\xi}{x-\xi} \quad (2.6)$$

by simple integration by parts, which immediately gives

$$\frac{dD_x}{dx} = \frac{1}{\pi} \left[\frac{p(\xi)}{x-\xi} \right]_{-\infty}^{\infty} + \frac{1}{\pi} \frac{d}{dx} \oint_{-\infty}^{\infty} \frac{p(\xi)d\xi}{x-\xi} . \quad (4.16)$$

At any finite value of x the first term in the right hand side of equation (4.16) is seen to identically vanish and equation (4.16) can be straightforwardly integrated to produce equation (4.15). In order to use equation (4.15) in the second sweep of the present scheme, this is first written in finite difference form as

$$\frac{D_i^{n+1} - D_{i-1}^{n+1}}{\Delta x} = \frac{1}{\pi} \oint_{x_1}^{x_I} \frac{pd\xi}{x-\xi} = CI(\bar{x}_i) . \quad (4.17)$$

Note that in equation (4.17) the finite difference representation for D_x^{n+1} is centered at the midpoint \bar{x}_i to avoid any differencing across the jump point. Also note that $CI(\bar{x}_i)$ is evaluated without any difficulties, since $p(\xi)$ is piecewise continuous throughout, and only once, at every location \bar{x}_i , for every $n+1$ time level. Equation (4.17) is then differenced once to give

$$\left(\frac{D_{i+1}^{n+1} - D_i^{n+1}}{\Delta x} - \frac{D_i^{n+1} - D_{i-1}^{n+1}}{\Delta x} \right) / \Delta x = \frac{CI(\bar{x}_{i+1}) - CI(\bar{x}_i)}{\Delta x} \quad (4.18)$$

which is conservative in nature and, therefore, exactly reproduces by integration the perfectly legitimate equation (4.17). Finally the relaxation integral

$\int_{\bar{x}_1}^{\bar{x}_{I-1}} \frac{D^{n+1} - 2D^* + D^n}{x - \xi} d\xi$ is added to the right hand side of

equation (4.18) to formally give

$$\frac{D_{i+1}^{n+1} - 2D_i^{n+1} + D_{i-1}^{n+1}}{\Delta x^2} = \frac{CI(\bar{x}_{i+1}) - CI(\bar{x}_i)}{\Delta x} + \int_{\bar{x}_1}^{\bar{x}_{I-1}} \frac{D^{n+1} - 2D^* + D^n}{x - \xi} d\xi \quad (4.19)$$

which is reduced to the tridiagonal form of equation (4.5) and inverted by Thomas Algorithm. The advantage of this alternate approach is in the evaluation of the Cauchy integral for the pressure, which has a regular behavior throughout.

It was found that the length of the region of integration for the pressure Cauchy integral was extremely critical to the convergence property of this method, and if the integration was limited to the region x_1, x_I as in the previous case, divergent behavior was invariably observed. The following analysis allows one to understand such behavior and obtain a favorable convergence property. In the previous numerical scheme the interaction law was effectively given by

$$D_{xx} = \frac{1}{\pi} \int_{x_1}^{x_I} \frac{p_\xi d\xi}{x - \xi} \quad (4.20)$$

Equation (4.20) gives by simple integration by parts

$$\frac{d}{dx}(D_x) = \frac{1}{\pi} \frac{d}{dx} \left[\int_{x_1}^{x_I} \frac{p(\xi) d\xi}{\bar{x}_i - \xi} + p(x_I) \ln(x_I - \bar{x}_i) - p(x_1) \ln(\bar{x}_i - x_1) \right] \quad (4.21)$$

Since $p(x_1) \equiv 0$ in the numerical scheme, its contribution to equation (4.21) is zero. $p(x_I)$ instead, even though very small, is $\neq 0$, and neglecting $p(x_I) \ln(x_I - \bar{x}_i)$ in equation (4.21) is numerically equivalent to introducing a "source term" in the numerical procedure, thus allowing the solution to grow without bound, i.e., to diverge. Simply adding $\frac{1}{\pi} p(x_I) \ln(x_I - \bar{x}_i)$ to the value of $CI(\bar{x}_i)$ given in equation (4.17) was found to eliminate the problem and to produce a convergent behavior (similar to the one typical of the previous scheme). This confirms the foregoing interpretation of the divergent behavior otherwise observed. It is believed that such a "source term effect" is the main cause of the convergence difficulties faced by many schemes using the interaction law, equation (4.15), (see for example Ref. 17), and that a proper accommodation of this problem could significantly improve their convergence property. For an interesting example of the importance of "source like terms" to the convergence of numerical relaxation techniques, see Ref. (31).

V. RESULTS

1. Supersonic Flow Results

The present algorithm as described in Section III was applied to the case of supersonic flow past a parabolic hump, for which solutions of the linearized equations are provided by Smith, (Ref. 8). The geometry of the hump in the nondimensional bottom deck variables is given in figures (1b and 2). The hump is located in the interval $0 \leq \theta x \leq 1$, where θ is Lighthill's constant ($\theta = 0.8272$) (Ref. 8). The hump profile is given by $hF(x) = \frac{hx(1-\theta x)}{\theta}$ in the interval $0 \leq \theta x \leq 1$; its maximum height is $\frac{h}{4\theta^2}$ corresponding to $\theta x = 0.5$. A small hump height ($h = 0.1$) was first taken into consideration in order to check the present scheme by direct comparison with Smith's linear results (Ref. 8). Figure (2) provides a comparison between the normalized wall shear and pressure obtained by the present numerical scheme for the nonlinear set of equations and Smith's linear solutions. The agreement is quite convincing and no other comparisons were sought. Step size studies have been performed in order to further confirm the reliability of the present method as well as verify its accuracy. Figures (3) and (4) present step size studies for normalized pressure and wall shear at the two most critical points, that is the leading and trailing edges of the hump ($\theta x = 0$ and $\theta x = 1$). As the results clearly indicate, the scheme is verified to be first order accurate

in the longitudinal x direction and second order accurate in the normal z direction. After that the reliability of the scheme was satisfactorily assessed by the comparisons and step size studies just presented, attention was devoted to hump heights of order one. In this case, since the full nonlinear set of equations only holds, a numerical solution is the only feasible one and is also the only means for assessing the occurrence of separation. Numerical results were obtained for values of h up to 6, for which separation and reattachment occur around the trailing edge of the hump. Figures (5), (6) and (7) present normalized wall shear, pressure and displacement thickness for values of h up to 4, compared with those corresponding to $h = 0.1$, in order to assess the influence of the nonlinearities on the solution profiles. As appears in figures (5) and (6) the effect of nonlinearity is seen to be as important for h increasing from 2 to 4 as for h increasing from 0.1 to 2, (which is reasonable) and the maximum deviations from the linear behavior occur in correspondence to the hump itself. Figure (7) shows the strange behavior (already anticipated in Section III) taken by the displacement function, which, as the total displacement ($\delta = D$ for $\theta x > 1$), tends to a nonzero asymptotic value as $x \rightarrow \infty$. Such behavior is due to truncation error and is a considerable entity since the scheme is only first order accurate in Δx . The insert of Figure (7) shows that at $\theta x = 2$ the value of δ extrapolated

to zero step size Δx is positive (not negative as appears in figure (7) and is therefore decaying as $x \rightarrow \infty$ as it should. Fortunately this improper behavior of δ for finite fairly large values of Δx does not influence the pressure and shear distributions which are related to the derivatives of the total displacement and are therefore not affected by the constant downstream shift of δ . The impact of non-linearity is also shown for the velocity profiles at three locations, leading edge, maximum height and trailing edge of the hump ($\theta x = 0, 0.5$ and 1). The $\frac{u-z}{h}$ (linear theory (Ref. 8) normalized longitudinal velocity) profiles are presented here for convenience in figure (8) for two values of h . The flow field is slightly decelerated at $\theta x = 0$, strongly accelerated at $\theta x = 0.5$ and strongly decelerated near the wall at $\theta x = 1$, where, for $h = 4$, the wall shear appears to be already negative. This is in agreement with physical expectation as well as linearized equations results.

Finally the total shear is shown in figure (9) to better display the large gradients and the wide variations for the shear which is seen to become negative, already for $h = 4$ and more so for $h = 6$, around the trailing edge of the hump. This confirms Smith's assumption, based on linear results, that the most likely place for separation to occur would indeed be at the backside of the hump (Ref. 8). Figure (9) also confirms the capability of the present scheme to properly assess separated flows. The results shown in

figures (4) through (9) have been obtained with a rather course mesh in both the x and z directions. They are believed to be qualitatively correct but only step size studies could reasonably assess their accuracy.

In the present study the outer edge boundary conditions were imposed at $z = 10$ for the smaller h values and $z = 15$ for the higher ones. In all cases it was numerically verified that the u velocity profile became linear ($u \rightarrow z - \delta$) over several mesh points below the outer edge. The upstream initial and downstream boundary conditions were set respectively at $x = -5$ and $x = 15$ and were numerically verified to be at a sufficient distance, since further increase of the region of integration produced no appreciable change in the results. The numerical procedure was found to converge (average absolute error on the total displacement height, $[\sum |D_i^{n+1} - D_i^n|] / (I-1), < 10^{-6}$) within 20 iterations (for h up to 1) and the computer time required for a typical case ($\theta \Delta x = 0.1$ $\Delta z = 0.25$, corresponding to 201 by 41 element matrices for the u and w velocities) was about 15 CPU seconds (AMDAHL 470 double precision arithmetic). The approximate optimal time step for convergence was numerically found to be given by $\lambda = 1$. In the presence of separation, convergence became slower and λ had to be increased up to 6 (for $h = 6$) to avoid divergent behavior. For the present geometry it is felt that $h = 6$ is close to the highest value of h for which the present scheme could converge because of the

horrendous gradients due to the geometry itself. The same scheme and a totally second order version of the same were also found to be very efficient for supersonic flow past a wedge. In this case convergence was easily obtained for normalized wedge angles up to 3, corresponding to a fairly large separation bubble and the results agreed very well with those of Refs. (13-15).

At the initial time level the pressure gradient and displacement thickness were taken equal to zero at all x_i locations in order to start the relaxation procedure. This physically corresponds to the introduction of the disturbing hump as time equals zero in an otherwise undisturbed uniform shear flow. For the higher hump cases, h was increased in gradual steps at every new time level t^n until the final value was reached. This was done in order to avoid divergent behavior produced by an otherwise too large time rate of change in the transient solution, which as already mentioned has no physical meaning anyway.

2. Subsonic Flow Results

The subsonic version of the present scheme as described in Section IV was applied to the solution of flow past the parabolic hump of figures (1b and 2) as well as the quartic hump of figure (1c). For the first case linearized equation results are provided by Smith (Ref. 8), whereas a numerical solution corresponding to a fairly large separation bubble is given by Sykes (Ref. 23) in the second case. The quartic

hump of figure (1c), whose profile is given by $hF(x) = h(1-x^2)^2$ for $-1 \leq x \leq 1$, has also the advantage of having continuous slope at its leading ($x = -1$) and trailing ($x = 1$) edges and therefore does not require any special numerical accommodation of the present algorithm at those locations. In both cases numerical solutions have been obtained by means of either numerical scheme discussed in Section IV.

Subsonic flow past the parabolic hump of figure (2) will be considered first. The small hump height, $h = 0.1$, has been again considered as a test case in order to compare the present numerical results with Smith's linear ones (Ref. 8). Figures (10) and (11) show the normalized wall shear and pressure profiles presently obtained compared with those of Ref. (8). Whereas a reasonable agreement is obtained for the case of the shear, the two pressure distributions show disturbing differences especially immediately upstream and downstream of the hump. Smith has kindly recalculated the pressure and shear profiles and his "improved" results are now indistinguishable from the present ones (Ref. 30). The present results given in figures (10) and (11) have been obtained by means of the second version of the algorithm (scheme B) described in Section IV. A longitudinal step size study has been performed in order to assess the accuracy and reliability of the solution technique. The results are given in figures (12) and (13) where wall shear and pressure

are seen to be first order accurate versus Δx at three different locations ($\theta x = 0, 0.5, 1$). Figure (13) is the more interesting in that it shows 2 different pressure results for each location x . The circles indicate the pressure values obtained by simple Euler quadrature of the pressure gradient distribution at the final time step $n+1$, after convergence has been reached. The squares indicate the values obtained by a second approach, exploiting the reciprocity property of the Riemann integrals. In fact, besides the interaction law equation (4.15)

$$D_x = \frac{1}{\pi} \oint_{-\infty}^{\infty} \frac{p_{\xi} d\xi}{x-\xi} , \quad (4.15)$$

the following conjugate integral expression is also true,

$$p = -\frac{1}{\pi} \oint_{-\infty}^{\infty} \frac{D_{\xi}}{x-\xi} d\xi . \quad (5.1)$$

Therefore, after the converged solution has been reached by means of the present numerical scheme, the pressure was evaluated by means of equation (5.1). The Cauchy integral (5.1) was evaluated by means of equation (B6) where D_{ξ} was replaced by a backward finite difference representation and the $D_{\xi\xi}$ correction was given by a central finite difference representation. The two different pressure evaluations are shown in figure (13) to be both first order accurate and at locations $\theta x = 0$ as well as $\theta x = 0.5$ they tend to the same limit values as Δx goes to zero. For $\theta x = 1$ the extrapolated results are slightly different and

this is probably due to the finiteness of the integration region for the Cauchy integrals as well as to the growth of the Goldstein layer originating at the leading edge of the hump (Ref. 15).

The effect of the finite Δz step was also investigated but it was found to be negligible at the level of $\Delta z = 0.2$ used in all present calculations. (It is worth remembering that the scheme is second order accurate in the normal z direction.)

The outer edge boundary conditions were imposed at $z = 8$ to 15 with increasing h . The range of integration in the longitudinal direction was taken to be $-5 \leq \theta x \leq 8$ and moving the range further upstream and downstream the two limits was seen to produce minor changes in the solution. Also, introducing the downstream far field asymptotic evaluation of the Cauchy integral residual as described in Appendix D was seen to modify the results by about two percent or less. Optimizing the procedure could probably have produced the same level of accuracy with a shorter numerical integration region but this aspect was not pursued further at the present time. All the results presented here have the Cauchy integral region of integration limited to the range $-5 \leq \theta x \leq 8$.

The approximate optimal time step for the subsonic algorithm was obtained for $\lambda = 2$ but again it had to be increased for the high h cases in order to avoid divergent

behavior. All the results presented here have been obtained by imposing a limit of ten to the number of iterations in the second sweep. The total procedure converged (average error of the total displacement $< 10^{-6}$) in about 50 to 80 time cycles for $h \leq 2$, depending on the value of the step size Δx (for lower values of Δx more iterations were needed). A typical calculation required about two to three minutes of computer time (AMDAHL 470, double precision arithmetic) a very small amount for a subsonic Triple-Deck solver. Convergence became very difficult for $h > 4$ and the need of further assessing the capability of the present scheme of handling reverse flow conditions irrespective of slope discontinuity singularities led to consideration of Sykes quartic hump (Ref. 23). The smooth nature of such a geometry (see figure 1c) also allowed the use of both schemes described in Section IV (and called schemes A and B for convenience) to provide a double check of the results. This was again obtained by means of a longitudinal step size study. Figure (16) shows the wall shear results obtained by both schemes at the 3 locations $x = -1, 0, 1$, for various values of Δx . The extrapolated results basically coincide to provide further credibility to the present approach. Figures (17) and (18) show the pressure values obtained by Euler's quadrature of the pressure gradient and by evaluation of the inverse Cauchy integral, equation (5.1), using schemes A and B respectively. Again all the extrapolated results

agree very well to prove once more the reliability of the numerical procedure. Figure (19) provides normalized wall shear and pressure distributions obtained for $h = 0.1$ by means of the first version of the algorithm, scheme A. For this case the outer boundary conditions were imposed at $z = 10$ and the region of integration was taken to be $-6 \leq x \leq 10$.

Finally the $h = 3$ case was considered in order to test the ability of the present scheme to handle the considerable reverse flow bubble anticipated by Sykes numerical predictions (Ref. 23). For this case convergence was very slow even when the Reyhner Flügge-Lotz approximation (Ref. 32) was used and the same phenomenon observed in Ref. (11) for the highest Reynolds number cases was encountered. The solution, while steadily converging everywhere else, presented an oscillatory behavior in time near the reattachment point, probably due to a source effect induced by the switching of the finite difference representation (forward-backward) of the longitudinal convective term. Upwinding the normal convective term was found somewhat helpful, and a way for completely eliminating such an oscillatory behavior around reattachment, was to set both convective terms equal to zero wherever the coefficient u (here taken as $(u_1^* + u_2^{*0})/2$) in the longitudinal convective terms uu_x of momentum equation (3.10) was found to be negative. Figures (20) and (21) show the shear and pressure profiles

obtained by introducing this approximation into the present scheme, as compared to Sykes numerical results (Ref. 23). The agreement is satisfactory if we consider that $\Delta x = 0.2$ in the present first order accurate scheme whereas, $\Delta x = 1/12$ in Sykes second order accurate scheme. More accurate solutions could not be obtained in this study because divergent behavior was observed for smaller values of the step size Δx . Such phenomenon is exactly equivalent to what was already encountered in high Re separated flow solutions of the interacting boundary layer equations in the vorticity stream function formulation (Ref. 11). Methods for correcting this divergent behavior are currently under investigation. Once the source of such "instabilities" is fully understood it is believed that accurate solutions for "high Reynolds number" separated flows will be feasible by means of the present Triple-Deck solver. Understanding this effect is also important in numerical solution of the Navier Stokes or interacting boundary layer equations since we have encountered the same difficulty there as well.

REFERENCES

1. Brown, S.N. and Stewartson, K. (1969), "Laminar Separation," Annual Review of Fluid Mechanics, 1, 45-72.
2. Stewartson, K. and Williams, P.G. (1969), "Self-Induced Separation," Proc. Roy. Soc., London, A 312, 181-206.
3. Stewartson, K. (1974), "Multistructured Boundary Layers on Flat Plates and Related Bodies," Advances in Applied Mechanics, Vol. 14, 146-239.
4. Sychev, V.Ya. (1972), "Concerning Laminar Separation," Izv. Akad. Nauk. SSSR, Mekh, Zhidk Gaza No. 3, 47-59.
5. Neiland, V.Ya. (1969), "Towards a Theory of Separation of the Laminar Boundary Layer in a Supersonic Stream," Izv. Akad. Nauk. SSSR, Mekh, Zhidk Gaza No. 4.
6. Neiland, V.Ya. (1971), "Flow Beyond the Separation Point of the Boundary Layer in Supersonic Stream," Izv. Akad. Nauk. SSSR, Mekh, Zhidk Gaza No. 3.
7. Messiter, A.F. (1970), "Boundary Layer Flow Near the Trailing Edge of a Flat Plate," S.I.A.M. J. Appl. Math., 18, 241-247.
8. Smith, F.T. (1973), "Laminar Flow Over a Small Hump on a Flat Plate," J. Fluid Mech., 57, 803-829.
9. Stewartson, K., (1970), "On Laminar Boundary Layers Near Corners," Q. J. Mech. Appl. Math., 23, 137; (1971) "Corrections and Addition," 24, 387.
10. Burggraf, O.R., Rizzetta, D., Werle, M.J. and Vatsa, V.N. (1977), "Effect of Reynolds Number on Laminar Separation of a Supersonic Stream," submitted to AIAA Journal for publication.
11. Napolitano, M., Werle, M.J. and Davis, R.T. (1978), "Numerical Solutions for High Reynolds Number Separated Flow," Presented at the AIAA 16th Aerospace Sciences Meeting, Huntsville, Alabama, January 16-18, 1978, AIAA Paper No. 78-56.
12. Williams, P.G. (1975), "A Reverse Flow Computation in the Theory of Self-Induced Separation," Proc. 4th Int. Conf. Num. Meths. in Fluid Dyn., Lecture Notes in Physics, Vol. 35, Springer-Verlag.
13. Jenson, R., Burggraf, O., Rizzetta, D. (1975), "Asymptotic Solution for Supersonic Viscous Flow Past a Compression Corner," Proc. 4th Int. Conf. Num. Meths. in Fluid Dyn., Lecture Notes in Physics, Vol. 35, Springer Verlag.

14. Rizzetta, D. (1976), "Asymptotic Solution for Two-Dimensional Viscous Supersonic and Hypersonic Flows Past Compression and Expansion Corners," Ph.D. Dissertation, The Ohio State University.
15. Jenson, R. (1977), "Numerical Solution of Weakly Separated Flows at High Reynolds Number," Ph.D. Dissertation, The Ohio State University.
16. Jobe, C.E. and Burggraf, O.R. (1974), "The Numerical Solution of the Asymptotic Equations of Trailing Edge Flow," Proc. Roy. Soc., London, A 340, 91-111.
17. Chow, R. and Melnik, R.E. (1976), "Numerical Solutions of the Triple-Deck Equations for Laminar Trailing-Edge Stall," Proc. 5th Int. Conf. Num. Meths. in Fluid Dyn., Lecture Notes in Physics, Vol. 59, Springer Verlag.
18. Messiter, A.F. and Enlow, R.L. (1973), "A Model for Laminar Boundary Layer Flow Near A Separation Point," S.I.A.M. Journal, 25, 655.
19. Smith, F.T. (1977), "The Laminar Separation of an Incompressible Fluid Streaming Past a Smooth Surface," Proc. Poy. Soc., London, A 356, 443-463.
20. Werle, M.J. and Vatsa, V.N. (1974), "A New Method for Supersonic Boundary Layer Separation," AIAA Journal, November, 1974, 1491-1497.
21. Rosenhead, L. (Ed.) (1966), Laminar Boundary Layers, Oxford University Press, Oxford.
22. Blottner, F.G. (1975), "Computational Techniques for Boundary Layers," AGARD Lecture Series No. 73, February 1975, pp. 3-9.
23. Sykes, R.I., "Stratification Effects in Boundary Layer Flow Over Hills," submitted to Proc. Roy. Soc., London.
24. Carnahan, B., Luther, H.A., and Wilkes, J.O. (1969), Applied Numerical Methods, John Wiley & Sons, Inc., New York.
25. Van Dyke, M.D. (1959), "Second Order Subsonic Airfoil Theory," NACA Report 1274.
26. Hess, J.L. and Smith, A.M.O. (1966), "Calculation of Potential Flow About Arbitrary Bodies," Progress in Aeronautical Sciences, Pergamon, New York, pp. 1-138.
27. Botta, E.F.F., Dijkstra, D. and Veldman, A.E.P. (1972), "The Numerical Solution of the Navier-Stokes Equations for Laminar, Incompressible Flow Past a Parabolic Cylinder," Journal of Eng. Math, Vol. 6, pp. 63-81.

28. Bristow, D.R. (1977), "Recent Improvements in Surface Singularity Methods For the Flow Field Analysis About Two-Dimensional Airfoils," AIAA Paper 77-641, presented at the AIAA III Computational Fluid Dynamics Conference, Albuquerque, N.M., June 27-28, 1977.
29. Dilley, A.D. (1976), "An Integral-Equation Solution Technique for Two-Dimensional Potential Flow Problems," University of Cincinnati, Dept. of Aerospace Engineering AFL Report No. 76-12-29, December 1976.
30. Smith, F.T. (1978), Private Communication.
31. Napolitano, M., Werle, M.J. and Davis, R.T., "A Note on Numerical Methods for Viscous Flows With Source Effects," to be published.
32. Reyhner, T.A. and Flügge-Lotz, I. (1968), "The Interaction of a Shock Wave With a Laminar Boundary Layer," Int. J. Nonlinear Mech., 3, p. 173.

APPENDIX A

INVERSION PROCEUDRE FOR THE * SWEEP FINITE

DIFFERENCE EQUATIONS

The two sets of infinite difference equations given by equations (3.11), (3.12) and (3.13), (3.14) are easily recognized to be of the form

$$w_j = w_{j-1} - \tilde{c}_j u_j - \tilde{c}_j u_{j-1} + d_j \quad (A1)$$

and

$$A_j u_{j-1} + B_j u_j + C_j u_{j+1} = H_j - a5_j w_j \quad (A2)$$

where the coefficients \tilde{c}_j through $a5_j$ can be immediately identified by direct comparison with equations (3.11) through (3.14). Such a coupled set of finite difference equations can be directly inverted (see Ref. 22) by means of the simple recursion relation

$$u_j = E_j u_{j-1} + \bar{F}_j + G_j w_{j-1} \quad (A3)$$

where the coefficients E_j , \bar{F}_j , G_j are given at location j by the following equations.

$$E_j = \frac{-A_j + (C_j G_{j+1} + a5_j) \tilde{c}_j}{[B_j + C_j E_{j+1} - (C_j G_{j+1} + a5_j) \tilde{c}_j]} \quad , \quad (A4)$$

$$F_j = \frac{H_j - C_j \bar{F}_{j+1} (C_j G_{j+1} + a5_j) d_j}{[B_j + C_j E_{j+1} - (C_j G_{j+1} + a5_j) \tilde{c}_j]} \quad , \quad (A5)$$

and

$$G_j = - \frac{C_j G_{j+1} + a5_j}{[G_j + C_j E_{j+1} \quad (C_j G_{j+1} + a5_j) \tilde{c}_j]} \quad (A6)$$

The complete solution for the two arrays u_j and w_j can be directly obtained by means of equations (A1) and (A3) once the wall values u_1 and w_1 are known together with all the coefficients E_j , F_j , G_j . The values u_1 and w_1 are directly provided by the wall boundary conditions which in this case are $u_1 = w_1 = 0$ (see equations (3.16) for comparison). The coefficients E_j , \bar{F}_j , G_j can be obtained by means of equations (A4) through (A6) once their values at the last grid point z_J are known. These are determined by means of the outer edge boundary condition equations (3.18) or (3.19) as described below. The last three points in the computational mesh are indicated for simplicity as 3, 2, 1 (see figure A1) and the following second order representations of the longitudinal velocity u at points 2 and 1 are written by means of Taylor series expansions:

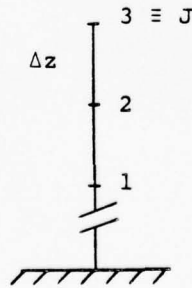


Figure A1. Boundary Condition Treatment.

$$u_2 = u_3 - \Delta z u_3' + \frac{\Delta z^2}{2} u_3'' + O(\Delta z^3) \quad (A7)$$

and

$$u_1 = u_3 - 2\Delta z u_3' + 2\Delta z^2 u_3'' + O(\Delta z^3) \quad (A8)$$

(Note that ' indicates here partial differentiation with respect to z.) By replacing u_3' by its known value χ ($\chi = 0$ or 1) and eliminating u_3'' in equations (A7) and (A8), the following second order accurate relation for the values of u at the three locations of figure A1 is obtained

$$u_1 = 4u_2 - 3u_3 + 2\chi\Delta z \quad (A9)$$

The finite difference equation (A2) is then written at grid point 2 to give

$$A_2 u_1 + B_2 u_2 + C_2 u_3 = H_2 - a_5 w_2 \quad (A10)$$

which, after eliminating u_1 by means of equation (A9), can be written as

$$u_3 = - \frac{B_2 - 4A_2}{C_2 - 3A_2} u_2 + \frac{H_2 - 2\chi A_2 \Delta z}{C_2 - 3A_2} - \frac{a_5 w_2}{C_2 - 3A_2} \quad (A11)$$

Note that equation (A11) is nothing else but the recursion formula (A3), written at the last grid point, $3 \equiv J$, and provides the sought after relations for the coefficients E_3 , \bar{F}_3 , G_3 , namely

$$E_3 = - \frac{B_2 - 4A_2}{C_2 - 3A_2} \quad (A12)$$

$$\bar{F}_3 = \frac{H_2 - 2\chi A_2 \Delta z}{C_2 - 3A_2} , \quad (A13)$$

and

$$G_3 = \frac{-a5_2}{C_2 - 3A_2} . \quad (A14)$$

The complete inversion procedure described in this Appendix is performed by a subroutine which receives from the main program all the arrays \tilde{c}_j through $a5_j$ and the appropriate value of χ (0 or 1) and returns to the main program the solution arrays u_j, w_j indicating here U_j, W_j or \tilde{u}_j, \tilde{w}_j respectively.

APPENDIX B

NUMERICAL SOLUTION OF CAUCHY INTEGRALS

The problem considered here is the numerical evaluation of a Cauchy integral of the type

$$CI(x) = \oint_a^b \frac{f(\xi) d\xi}{x-\xi} \quad \text{for } a < x < b \quad (B1)$$

where $f(\xi)$ is a piecewise continuous function in the interval a, b .

In order to numerically evaluate $CI(x)$, the interval of integration a, b is divided into an arbitrary number of equally spaced grid points x_i ($i = 1, 2, \dots, I$) such that $x_1 = a$ and $x_I = b$. The midpoints of each grid are also important and are indicated as \bar{x}_i ($\bar{x}_i = x_i + \frac{\Delta x}{2}$, $i = 1, 2, \dots, I-1$).

$CI(x)$ can be numerically evaluated at any location \bar{x}_i by the following expression,

$$CI(\bar{x}_i) = \sum_{j=1}^{I-1} f(\bar{x}_j) \oint_{x_j}^{x_{j+1}} \frac{d\xi}{\bar{x}_i - \xi} = \sum_{j=1}^{I-1} f(\bar{x}_j) \frac{1}{2} \ln \left(\frac{\bar{x}_i - x_j}{\bar{x}_i - x_{j+1}} \right)^2, \quad (B2)$$

or, to the same order of accuracy,

$$CI(\bar{x}_i) = \sum_{j=1}^{I-1} \frac{f(x_j) + f(x_{j+1})}{2} \frac{1}{2} \ln \left(\frac{\bar{x}_i - x_j}{\bar{x}_i - x_{j+1}} \right)^2. \quad (B3)$$

Note that equations (B2) or (B3) correspond to the simple trapezoidal rule in which the function $f(\xi)$ has been averaged over each mesh of the integration domain and the

remaining term $d\xi/(x-\xi)$ has been analytically integrated over each grid to properly account for the Cauchy principal value nature of the integral $CI(x)$. Therefore, the accuracy of equations (B2) and (B3) might be expected to be second order versus Δx . However, application of equation (B3) to the following model problem,

$$CI(x) = \oint_{-1}^1 \frac{\xi^2}{x-\xi} d\xi = x(x \ln \frac{1+x}{1-x} - 2) \quad (B4)$$

(Ref. 25), produced only first order accurate solutions. Figure 22 clearly shows that $CI(0.45)$ as well as $CI(-0.15)$ evaluated by means of equation (B3) linearly approach the exact analytical values (in the limit of zero step size, Δx). In general, a first order accurate numerical integration is able to exactly reproduce the analytical value of the sought after integral only for a constant value of the integrand (Ref. 24). In the present special case then, equation (B2) should be able to provide the exact solution for $\oint_a^b \frac{f(\xi)dx}{x-\xi}$ only if $f(\xi)$ is a constant in any interval $x_j - x_{j+1}$. This was numerically verified for the following model problem, $\oint_{-1}^1 \frac{d\xi}{x-\xi} = x \ln \frac{1+x}{1-x} - 2$, (Ref. 25). The numerical integration scheme provided by equation (B2) or (B3) as well, is therefore only first order accurate and such an apparently anomalous result needs further analysis. A first understanding of such behavior can be obtained by noting that in equation (B2) or (B3) the integration across the step $x_i - x_{i+1}$ (in which the argument

of $CI(\bar{x}_i)$ becomes singular) gives zero contribution to the integral itself. However, the exact contribution to the total integral $CI(\bar{x}_i)$ due to the integration across such an interval is zero indeed only if the function $f(\xi)$ is even around \bar{x}_i , the midpoint of the interval itself. In general, instead, it might be reasonably expected to be of order Δx , the length of the interval itself. Neglecting such contribution could therefore be sufficient to produce the first order accurate behavior of the present scheme. The above argument received numerical support by the solution of the following integral

$$CI_1(x) = \int_{-1}^1 \frac{(\xi - 0.45)^2 d\xi}{x - \xi}, \quad (B5)$$

obviously chosen because, in light of the foregoing discussion, equation (B2) or (B3) should provide a second order accurate solution for $CI_1(0.45)$ whereas only a first order accurate one for $CI_1(x)$ at any other location $x \neq 0.45$. Figure 23 shows that this is indeed the case, thus supporting the previous discussion. A complete understanding of the problem will be shortly obtained by analyzing a general second order accurate integration scheme for equation (B1), provided below. Such a second order scheme should be able to resolve the previously discussed anomaly and also to reproduce the exact analytical value of $CI(x)$ for any piecewise linearly varying function $f(\xi)$. This can be easily accomplished by extracting the

average values of the function $f(\xi)$ and its first derivative over every integration mesh interval, analytically integrating the remaining part of the integrand to properly account for its singular nature, and finally summing all these contributions in the following way:

$$\begin{aligned}
 CI(\bar{x}_i) &= \oint_a^b \frac{f(\xi)}{\bar{x}_i - \xi} d\xi = \sum_{j=1}^{I-1} \oint_{x_j}^{x_{j+1}} \frac{f(\xi) d\xi}{\bar{x}_i - \xi} \\
 &= \sum_{j=1}^{I-1} \frac{f(x_{j+1}) + f(x_j)}{2} \oint_{x_j}^{x_{j+1}} \frac{d\xi}{\bar{x}_i - \xi} + \sum_{j=1}^{I-1} \frac{f(x_{j+1}) - f(x_j)}{\Delta x} \oint_{x_j}^{x_{j+1}} \frac{\xi - \bar{x}_j}{\bar{x}_i - \xi} d\xi \\
 &= \sum_{j=1}^{I-1} \frac{f(x_{j+1}) + f(x_j)}{2} \frac{1}{2} \ln \left(\frac{\bar{x}_i - x_j}{\bar{x}_i - x_{j+1}} \right)^2 \\
 &\quad + \sum_{j=1}^{I-1} \frac{f(x_{j+1}) - f(x_j)}{\Delta x} [(\bar{x}_i - \bar{x}_j) \oint_{x_j}^{x_{j+1}} \frac{d\xi}{x - \xi} - \int_{x_j}^{x_{j+1}} d\xi];
 \end{aligned}$$

finally,

$$\begin{aligned}
 CI(x_i) &= \sum_{j=1}^{I-1} \frac{f(x_{j+1}) + f(x_j)}{2} \frac{1}{2} \ln \left(\frac{\bar{x}_i - x_j}{\bar{x}_i - x_{j+1}} \right)^2 \\
 &\quad + \sum_{j=1}^{I-1} \frac{f(x_{j+1}) - f(x_j)}{\Delta x} [(\bar{x}_i - \bar{x}_j) \frac{1}{2} \ln \left(\frac{\bar{x}_i - x_j}{\bar{x}_i - x_{j+1}} \right)^2 - \Delta x] .
 \end{aligned} \tag{B6}$$

Note that equation (B6) essentially contains the same term as equation (B3) plus corrections proportional to the local slope of the function $f(\xi)$, $[f(x_{j+1}) - f(x_j)]/\Delta x = f'(\bar{x}_j) + O(\Delta x^2)$. Such a contribution, for the case $(i-j) \neq 1$, can be written as

$$f'(\bar{x}_j) [(i-j)\Delta x \ln \frac{2(i-j)-1}{2(i-j)+1} - \Delta x] + O(\Delta x^2) \quad (B7)$$

and is easily seen to be a first order correction. Equations (B6) and (B7) also show that if $f(\xi)$ is even ($f'(\xi)$ odd) around the \bar{x}_j location, the first order terms exactly cancel each other, thus producing the second order accurate behavior observed in Figure 23. Equation (B7) further shows that the dominant $O(\Delta x)$ contributor is due to the step size containing the singularity, as previously anticipated. In fact, for $(i-j) \neq 1$, Equation (B7) gives, by Taylor series expansion in terms of the "small parameter" $1/(i-j)$,

$$f'(\bar{x}_j) [\Delta x (\frac{i-j}{i-j} + \text{H.O.T.}) - \Delta x] + O(\Delta x^2) , \quad (B8)$$

which is seen to be a "small" $O(\Delta x)$ contribution. For $i = j$, Equation (B7) gives instead,

$$(-f'(\bar{x}_j) + \text{H.O.T.}) \Delta x + O(\Delta x^2) , \quad (B9)$$

which is the main first order contribution neglected by equation (B2) or (B3), whose first order accurate behavior is now completely understood.

It is important to mention that in equation (B6) the group $\frac{f(x_j) + f(x_{j+1})}{2}$ can be replaced by $f(\bar{x}_j)$ and the one $\frac{f(x_{j+1}) - f(x_j)}{\Delta x}$ by $\frac{f(\bar{x}_{j+1}) - f(\bar{x}_{j-1})}{2\Delta x}$, to produce four second order accurate schemes. Here two of them, namely the one

given in equation (B6) and that obtained with both the above indicated modifications, have been applied to the model problem, equation (3), and are shown to recover the exact solution with second order accurate behavior in figure 24. They also have been able to reproduce the exact analytical solution for the problem,

$\oint_{-1}^1 \frac{\xi}{x-\xi} d\xi = x \ln \frac{1+x}{1-x} - 2$, (Ref. 25), for any of the step sizes used for the results of figure 24, thus confirming once more their second order accurate nature.

It must be acknowledged that the present technique is a special application of more general methods for computing two dimensional potential flows about arbitrary bodies by means of source and or vortex singularity distribution (see Refs. 26, 27, 28). Dilley, for example, has already used generalized expressions of equation (B6) (Ref. 29). His failure of achieving second order accuracy is most probably due to the curved nature of the bodies considered in his study or to the variable step size of his computational domain.

APPENDIX C
A VECTORIZATION OF LOGARITHMS IN THE
CAUCHY INTEGRAL SOLVER

It has been seen in Appendix B that an extremely large number of logarithms must be computed in order to evaluate the Cauchy integrals of the subsonic interaction law, equation (2.6). Such logarithms are of the form

$$AL_{i,j} = \frac{1}{2} \ln \left(\frac{\bar{x}_i - x_j}{\bar{x}_i - x_{j+1}} \right)^2 \quad (C1)$$

with $2 \leq i \leq I-1$, $2 \leq j \leq I-1$, and could be easily calculated once and for all and stored in a square matrix of order $I-2$, to avoid the extremely large computational effort of evaluating them when they are needed. It is worth mentioning that for every iteration in the second sweep of the numerical procedure described in Section IV, the single operation of equation (C1) is performed $(I-2)^2$ times. Considering that such second sweep calculations can be performed up to a 1000 times ($10 * 100$) and that logarithmic calculations are extremely time consuming on the computer, it is easy to understand the great need of calculating equation (C1) once and for all. The use of a square matrix though requires large storage for small step size computations. It is sufficient to mention that for $(I-2) = 200$, a double precision evaluation

of $AL_{i,j}$ would require 320 Kilobytes of central memory, which would rise up to the prohibitive figure of 2000 for $(I-2) = 500$. Fortunately, a simple vector of $2I-3$ length can serve the purpose equally well, if a constant grid is used in the computational scheme. It is sufficient to observe that the argument of equation (C1) only depends on the relative distance between the points \bar{x}_i and \bar{x}_j (see figure C1).

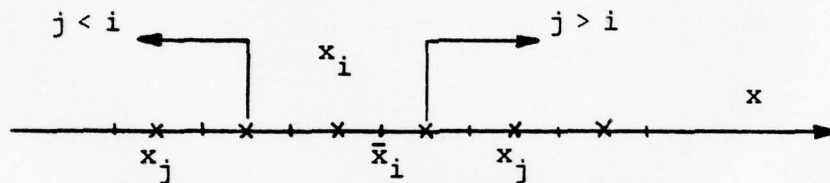


Figure C1. Grid Distribution.

If $(i-j) < 0$

$$AL_{i,j} = AL_k = \ln \left[\frac{(j-i)\Delta x - \Delta x/2}{(j-i)\Delta x + \Delta x/2} \right] = \ln \frac{2(j-i)-1}{2(j-i)+1}, \quad (C2)$$

if $(i-j) > 0$

$$AL_{i,j} = AL_k = \ln \frac{2(i-j)+1}{2(i-j)-1}, \quad (C3)$$

and finally, if $(i-j) = 0$

$$AL_{i,j} = AL_k = 0. \quad (C4)$$

It is sufficient to calculate once and for all the values of equations (C2) through (C4) and store them in the vector AL_k . For $k = I$, $AL = 0$ and for $I+1 < k < 2I-1$,

AL_k will contain the values corresponding to $(i-j) > 0$,
 whereas for $1 < k < I$, AL_k will contain the values
 corresponding to $(i-j) < 0$. It is sufficient to define
 $k = I + i-j$, and the correct value ($AL_k = AL_{i,j}$) will be
 immediately available whenever necessary. Fortran
 programming of this procedure is straightforward and
 very short. Its use has produced considerable saving of
 computing effort. (For a case in which 2 minutes of
 AMDAHL 470 are presently used, repetitive calculation of
 the logarithms led to a total computational effort of
 10 minutes.)

Finally, it must be noted that the vector AL_k is
 symmetric around its central element AL_I and properly
 exploiting such a property could lead to a further
 reduction of the computer storage from $2I-3$ to just $I-1$
 double precision locations. Considering though the more
 elaborate logic and the larger computational effort
 needed to implement such a procedure, the present approach
 is definitely the simplest and most efficient one.

APPENDIX D

ANALYTICAL EVALUATION OF FAR FIELD ASYMPTOTIC CONTRIBUTION TO THE CAUCHY INTEGRALS

The problem of interest here is the evaluation of an integral of the type

$$\int_{-\infty}^{x_1} \frac{f(\xi) d\xi}{x-\xi} \quad \text{for } x > x_1, \quad (D1)$$

$$\int_{x_I}^{\infty} \frac{f(\xi) d\xi}{x-\xi} \quad \text{for } x < x_I. \quad (D2)$$

Note that in equations (D1) and (D2), the Cauchy principal value sign is missing because the argument becomes singular outside the interval of integration. An accurate evaluation of the integrals (D1) and (D2) is desirable, due to the slow algebraic decay of $f(\xi)$ as $\xi \rightarrow +\infty$ or as $\xi \rightarrow -\infty$ in most Triple-Deck equation applications. In this appendix only the solution of equation (D2) will be considered, for a function $f(\xi)$ decaying, as $\xi \rightarrow +\infty$, with a negative integer power law. This, because for subsonic flow past a hump the pressure gradient asymptotic decay is given (Ref. 8) as:

$$\frac{dp}{dx} \equiv f(\xi) \approx k \xi^{-3} \quad (\text{for } \xi \gg 1). \quad (D3)$$

Extension to larger values of the exponent is straightforward. The particular integral of interest is then

$$I(x) = k \int_{x_I}^{\infty} \frac{d\xi}{(x-\xi)\xi^3} . \quad (D4)$$

A simple change of variable of integration produces

$$I(x) = \frac{k}{x^3} \int_{x_I/x}^{\infty} \frac{d\eta}{(1-\eta)\eta^3} , \quad (D5)$$

and the integral of equation (D5) can be solved by the method of partial fractions. In fact, since

$$\frac{1}{\eta^3(1-\eta)} = \frac{1}{\eta^3} + \frac{1}{\eta^2} + \frac{1}{\eta} + \frac{1}{1-\eta} ,$$

$$I(x) = \frac{k}{x^3} \left[\frac{-1}{2\eta^2} - \frac{1}{\eta} + \ln \eta - \ln(\eta-1) \right]_{x_I/x}^{\infty} . \quad (D6)$$

Equation (D6) is only valid for $x > 0$, and a very similar one should be derived for $x < 0$. Simple regrouping of the logarithmic terms, though, produces the following final expression for $I(x)$, which is easily verified to be valid for negative as well as positive values of x

$$\frac{I(x)}{k} = \frac{1}{x^3} \left[\ln \left(\frac{x_I - x}{x_I} \right) + \frac{x}{x_I} + \frac{1}{2} \left(\frac{x}{x_I} \right)^2 \right] . \quad (D7)$$

Note that x_I is the lower limit of integration and has to be large enough to guarantee a satisfactory accuracy for the asymptotic representation of $f(\xi)$, equation (D3). x , instead, is the variable point at which the integral $I(x)$ is evaluated and can vary within the interval

$x_l < x < x_I$. A special treatment is of course required for $x = 0$. In this case the integration trivially produces

$$I(x)/k = \int_{x_I}^{\infty} \frac{d\xi}{-\xi^4} = -\frac{1}{3x_I^3} \quad . \quad (D8)$$

It is worth noting though that for $x \rightarrow 0$ and $\frac{x}{x_I} = \bar{\epsilon} \ll 1$ an asymptotic expansion, to third order, of the term $\ln(1-\bar{\epsilon})$ in equation (D7) identically reduces equation (D7) to equation (D8).

In practical problems, k must be determined by patching at every iteration the numerical solution around x_I with the asymptotic analytical expression (D3) for $f(\xi)$. A numerical account of expressions (D7) and (D8) is nevertheless extremely straightforward if x_I is fixed. The total right hand side of equations (D7) and (D8) is evaluated once and for all at every grid point x_i and stored in a vector for successive use.

APPENDIX E

CAUCHY INTEGRAL OF A DISCONTINUOUS FUNCTION

Given a function $f(x)$, discontinuous across the point $x = 0$ (for convenience) the value of the following integral

$$CI(x) = \int_{-a}^a \frac{f(\xi) d\xi}{x - \xi} \quad (E1)$$

at the point of discontinuity $x = 0$ is looked for. Since $CI(x)$ will be seen to become singular at $x = 0$ because of the discontinuity of $f(x)$ at the same location, the function $f(x)$ is taken for simplicity to be a constant R for $x < 0$ and a different constant S for $x > 0$, (see figure E1)

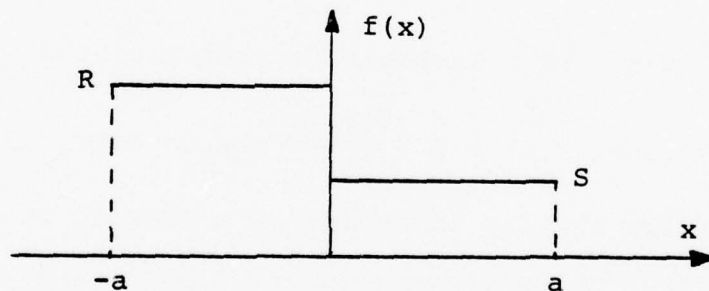


Figure E1. Discontinuous, Piecewise Constant Function.

$I(0)$ can then be easily evaluated by simply applying the definition of Cauchy principal value:

$$\begin{aligned} CI(0) &= \oint_{-a}^a \frac{f(\xi) d\xi}{-\xi} = \lim_{\epsilon \rightarrow 0} \left[\int_{-a}^{-\epsilon} \frac{-R d\xi}{\xi} + \int_{\epsilon}^a \frac{-S d\xi}{\xi} \right] \\ &= \lim_{\epsilon \rightarrow 0} (R-S) \ln \frac{A}{\epsilon} \rightarrow \infty \end{aligned} \quad (E2)$$

In order to further verify the result (E2) and at the same time eliminate the indeterminacy of $f(x)$ at $x = 0$, a second function $f(x)$ is also considered, which is constant from $-a$ to $-b$, varies linearly from R to S in the interval $-b$ to b and is again constant from b to a (see figure E2)

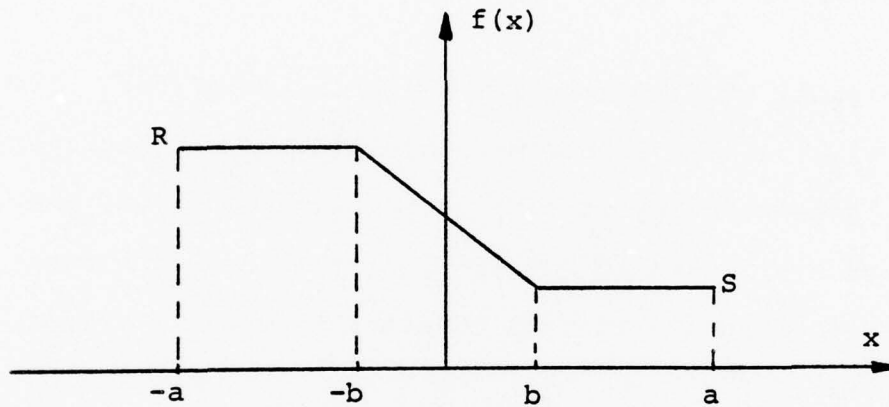


Figure E2. Linearly Varying Function.

For this case $I(0) = \oint_{-a}^a \frac{f(\xi)d\xi}{-\xi}$ can be easily determined analytically and its limit (for $b \rightarrow 0$) will produce the sought after discontinuous function result, as follows:

$$CI(0) = \oint_{-a}^a \frac{f(\xi)d\xi}{x-\xi} = \int_{-a}^{-b} \frac{-Rd\xi}{\xi} + \int_{-b}^b \left[\frac{(S-R)}{2b} - \frac{R+S}{2\xi} \right] d\xi + \int_b^a \frac{-Sd\xi}{\xi},$$

$$CI(0) = S-R + (R-S) \ln \frac{a}{b}, \quad (E3)$$

and

$$\lim_{b \rightarrow 0} CI(0) = \lim_{b \rightarrow 0} (R-S) \ln \frac{a}{b} = \lim_{\varepsilon \rightarrow 0} (R-S) \ln \frac{a}{\varepsilon} \rightarrow \infty . \quad (E4)$$

If the function $f(x)$ is allowed to vary linearly in the ranges $-a$, $-b$, and b , the basic result does not change and the Cauchy integral $CI(x)$ becomes infinite as $x \rightarrow 0$ like $\Delta f \ln|x|$, (where $\Delta f = S - R$, is the jump in $f(x)$). If $CI(x)$ is numerically evaluated by the second order Cauchy integral solver of Appendix A, the interval $-b$, b being equal to a step size Δx , equation (B6) will provide the exact analytical value of $CI(x)$ at any grid point x_i and for any Δx for a piecewise linear function $f(x)$. Furthermore, since such an exact result is given in terms of the same logarithms as the analytical one of equation (E3), it will also obviously produce the same limit value $\Delta f \ln \Delta x$ as $\Delta x \rightarrow 0$.

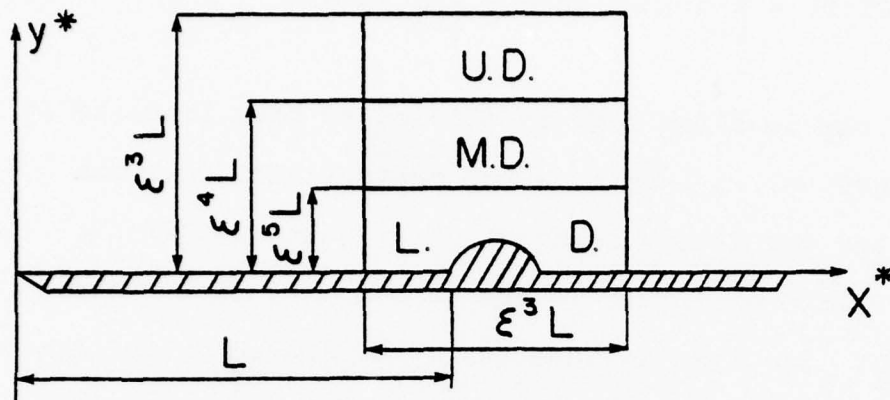


Fig. 1a. Triple-Deck Structure Around a Small Hump.

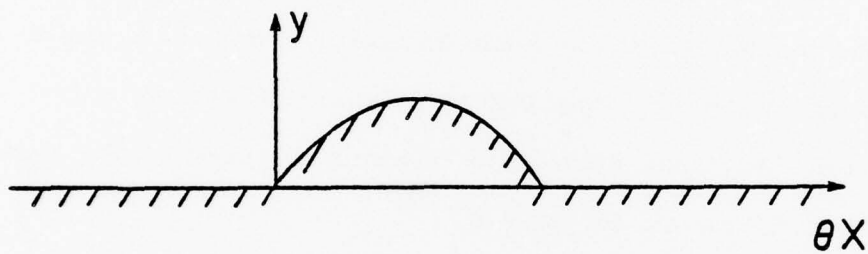


Fig. 1b. Parabolic Hump in Bottom Deck Scaling.

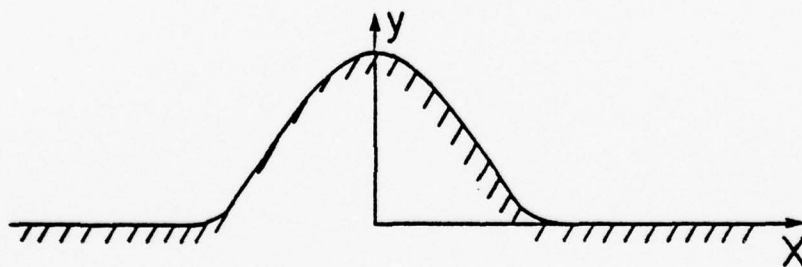


Fig. 1c. Quartic Hump in Bottom Deck Scaling.

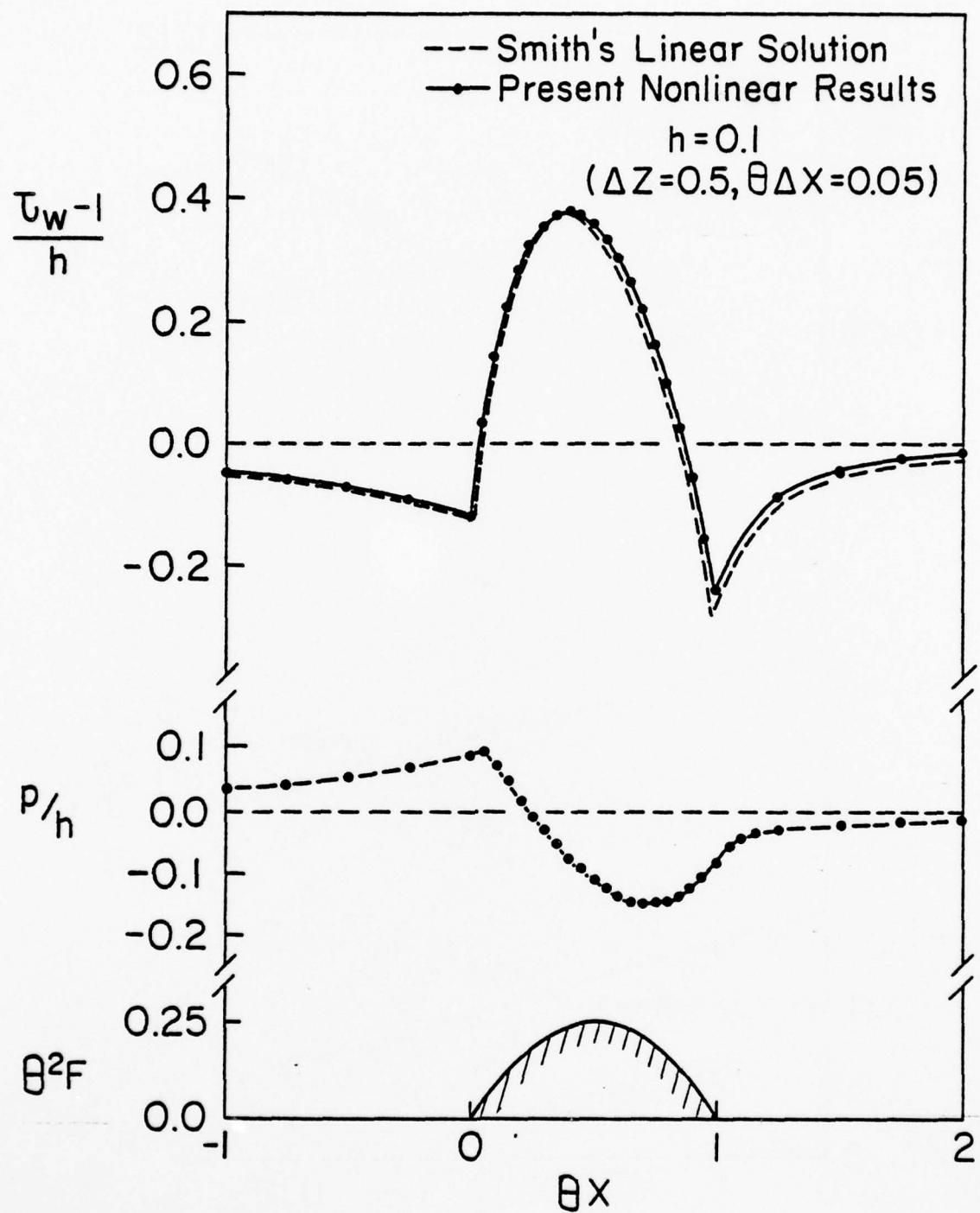


Fig. 2. Supersonic Flow Past a Parabolic Hump; Normalized Wall Shear and Pressure Profiles for $h = 0.1$.

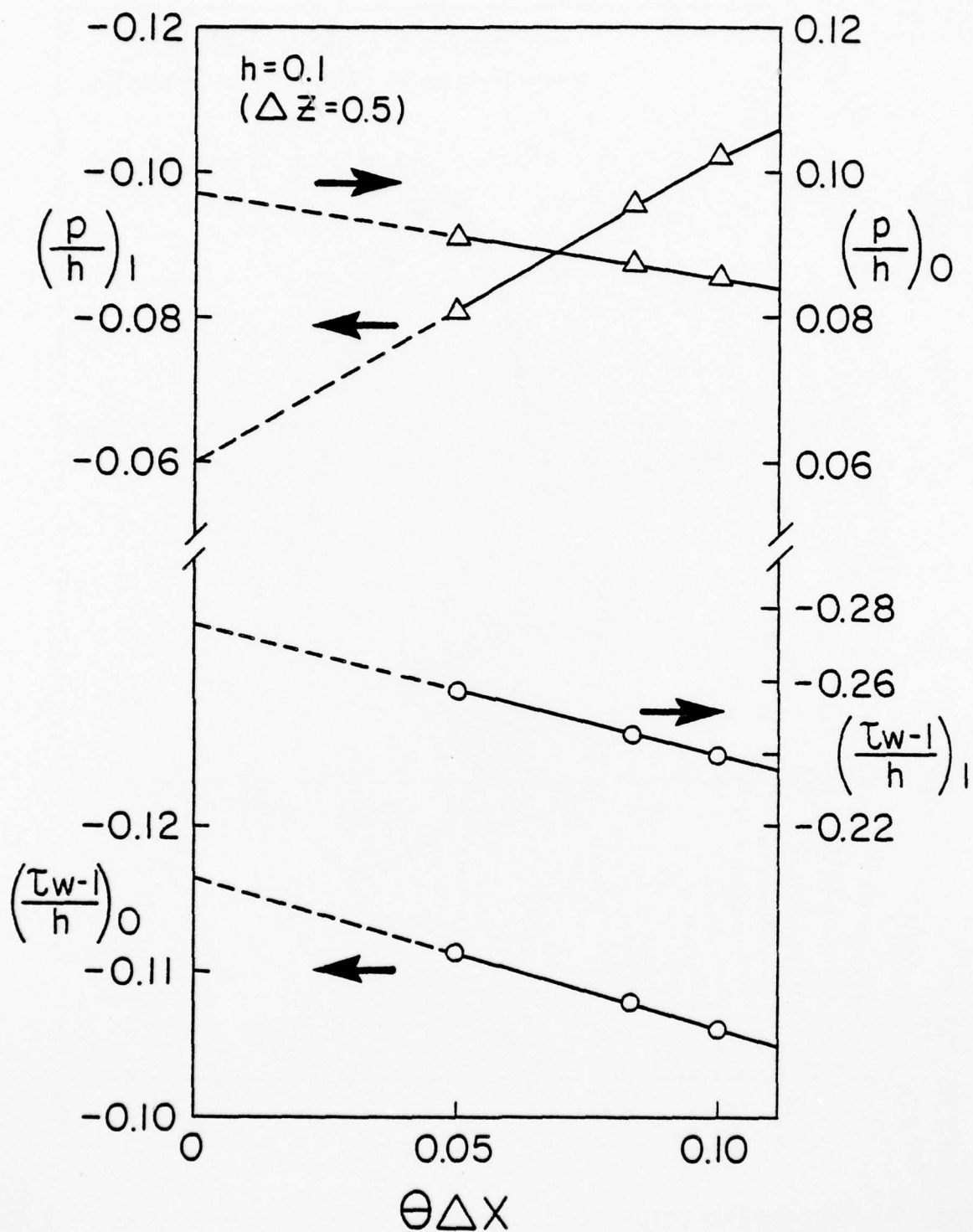


Fig. 3. Supersonic Flow Past a Parabolic Hump; Longitudinal Step Size Study.

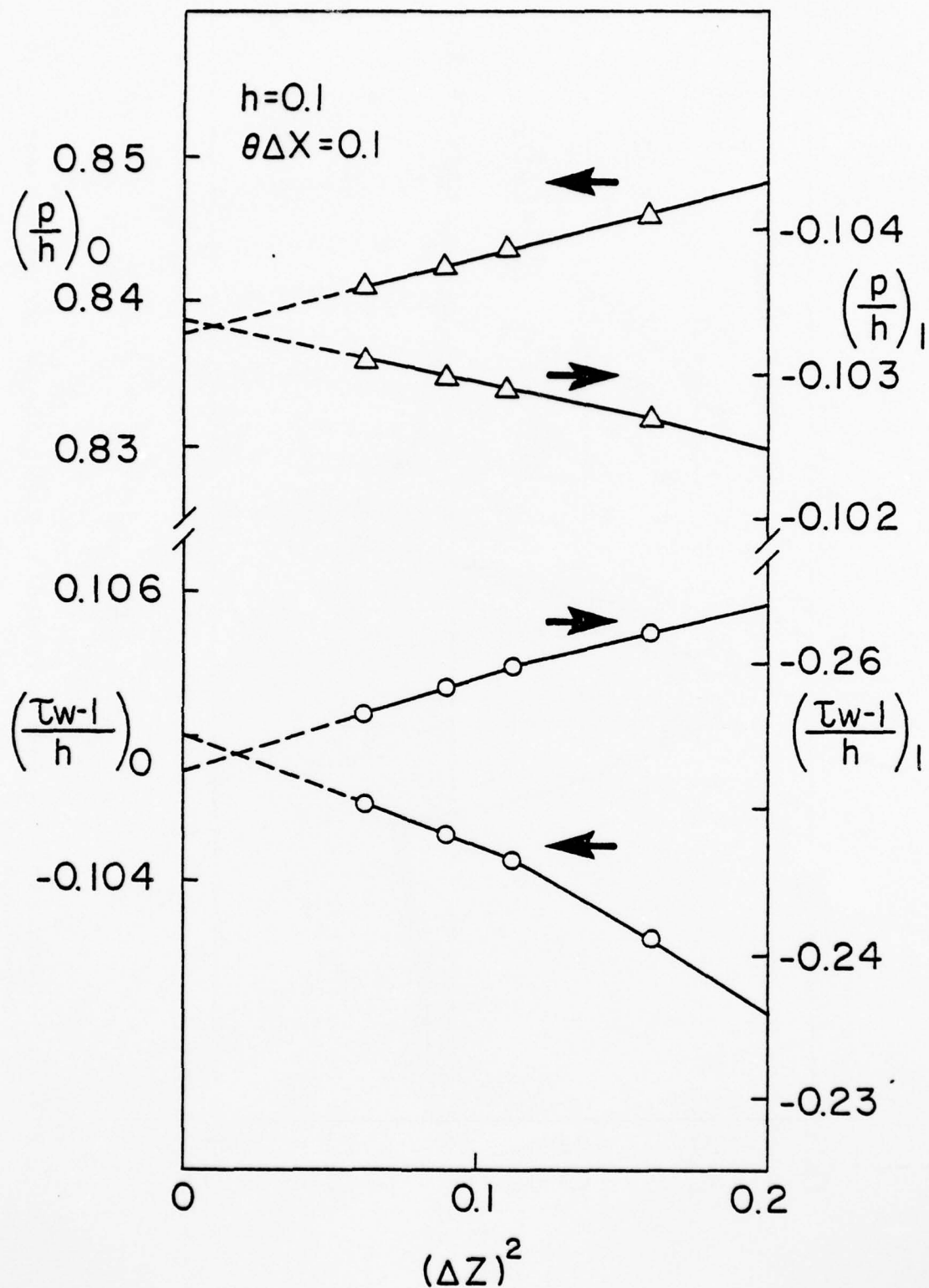


Fig. 4. Supersonic Flow Past a Parabolic Hump; Normal Step Size Study.

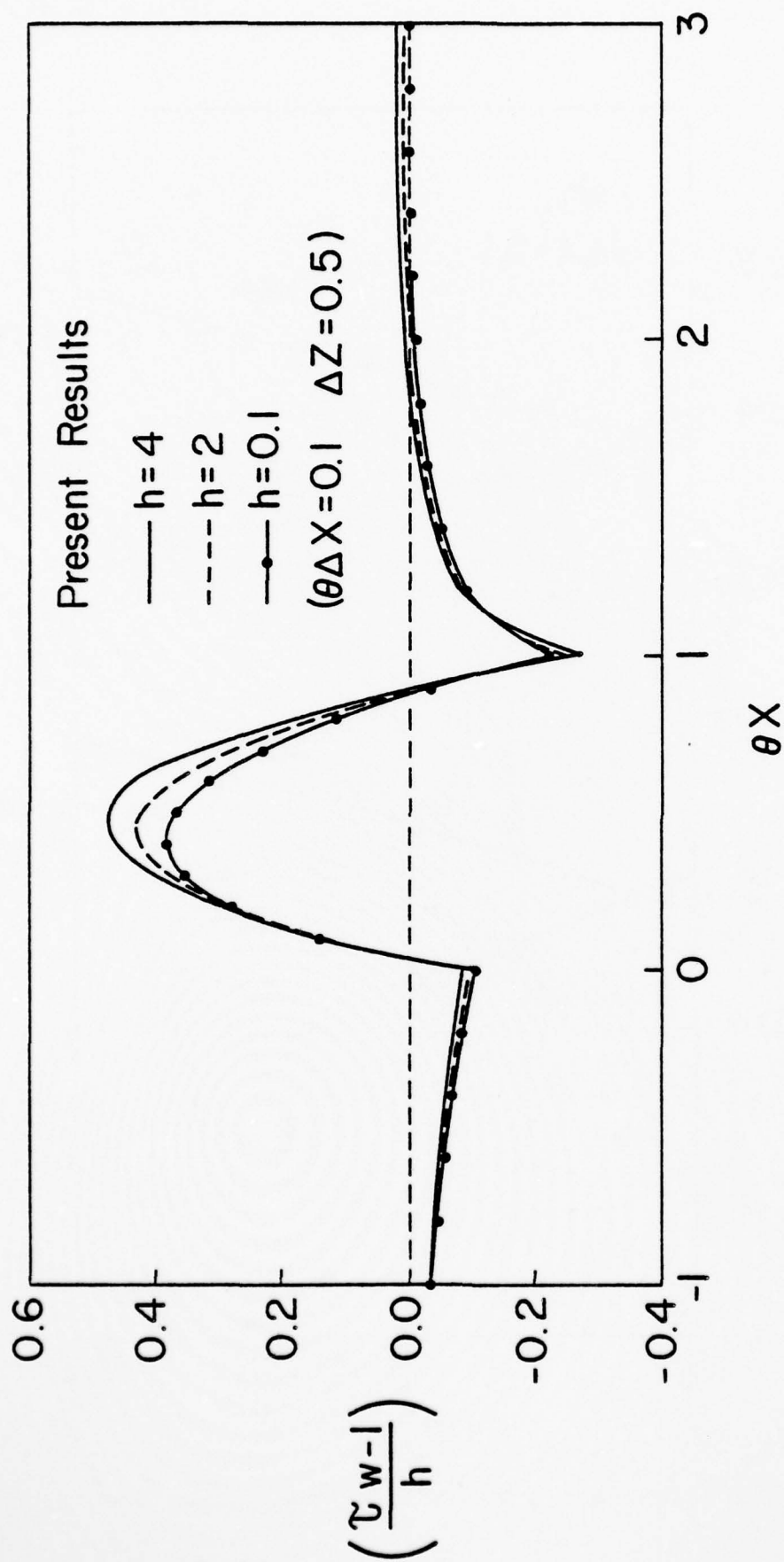


Fig. 5. Supersonic Flow Past a Parabolic Hump; Normalized Wall Shear Dependence on h .

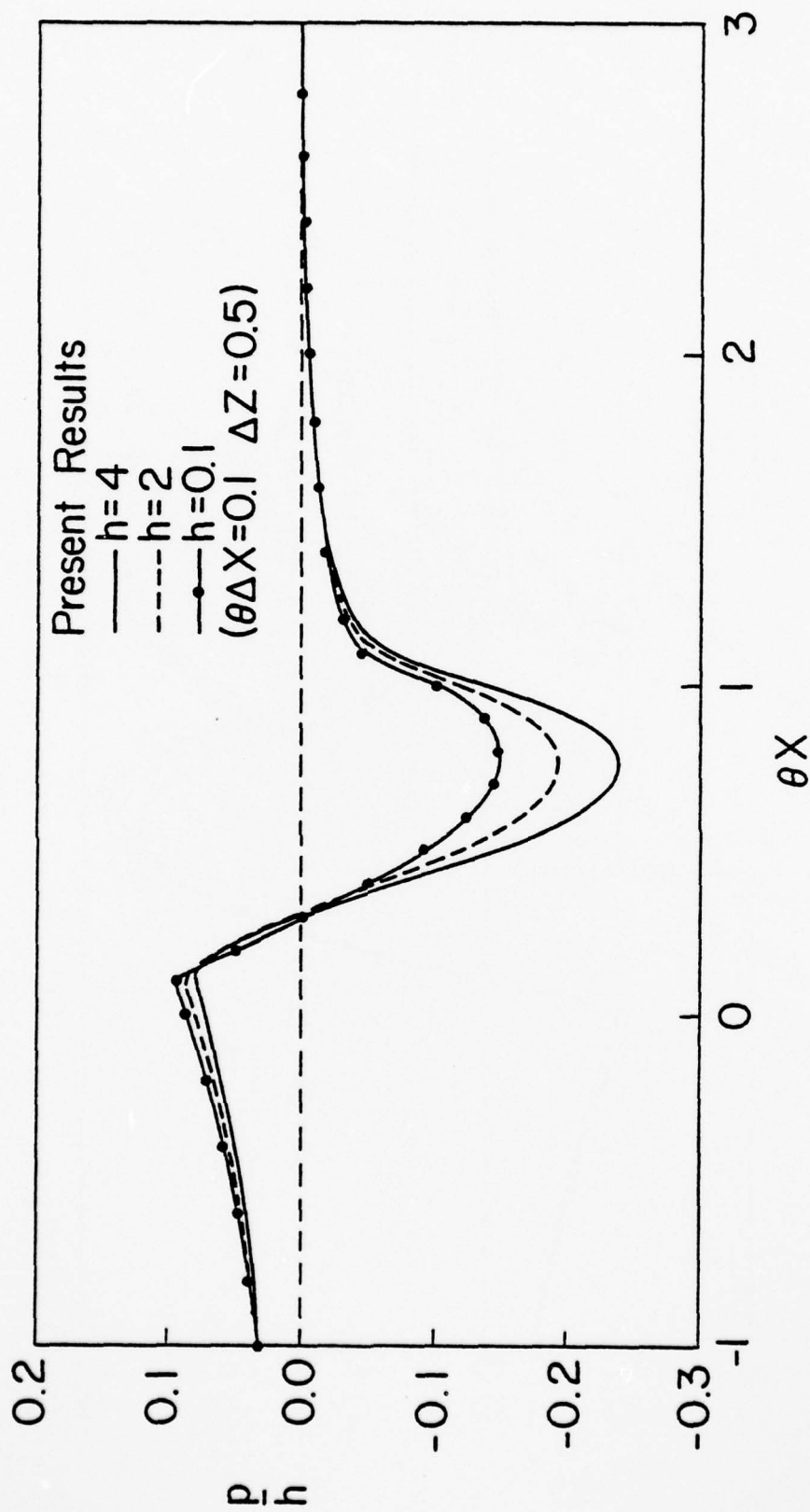


Fig. 6. Supersonic Flow Past a Parabolic Hump; Normalized Pressure Dependence on h .

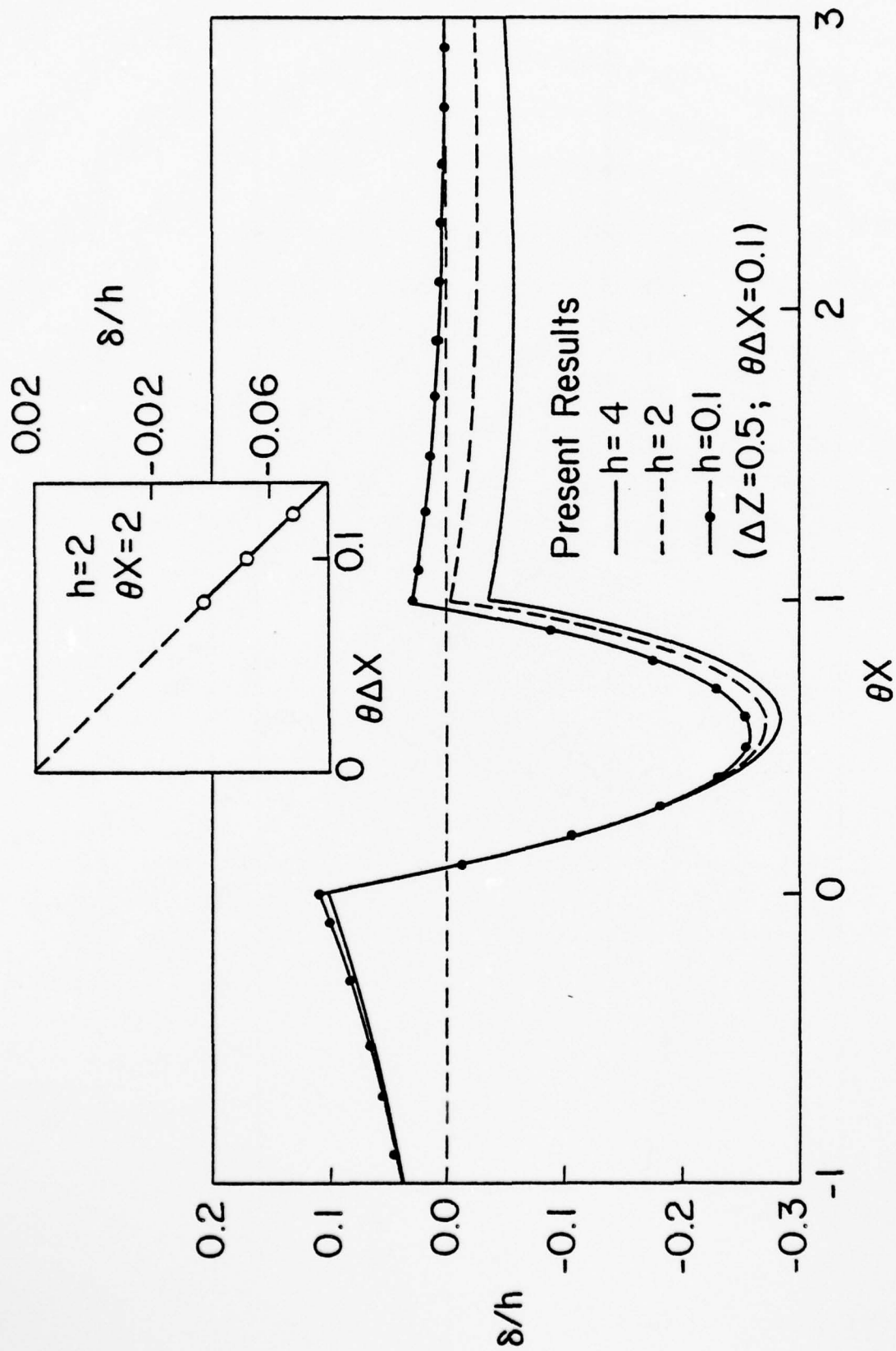


Fig. 7. Supersonic Flow Past a Parabolic Hump; Normalized Displacement Thickness Dependence on h .

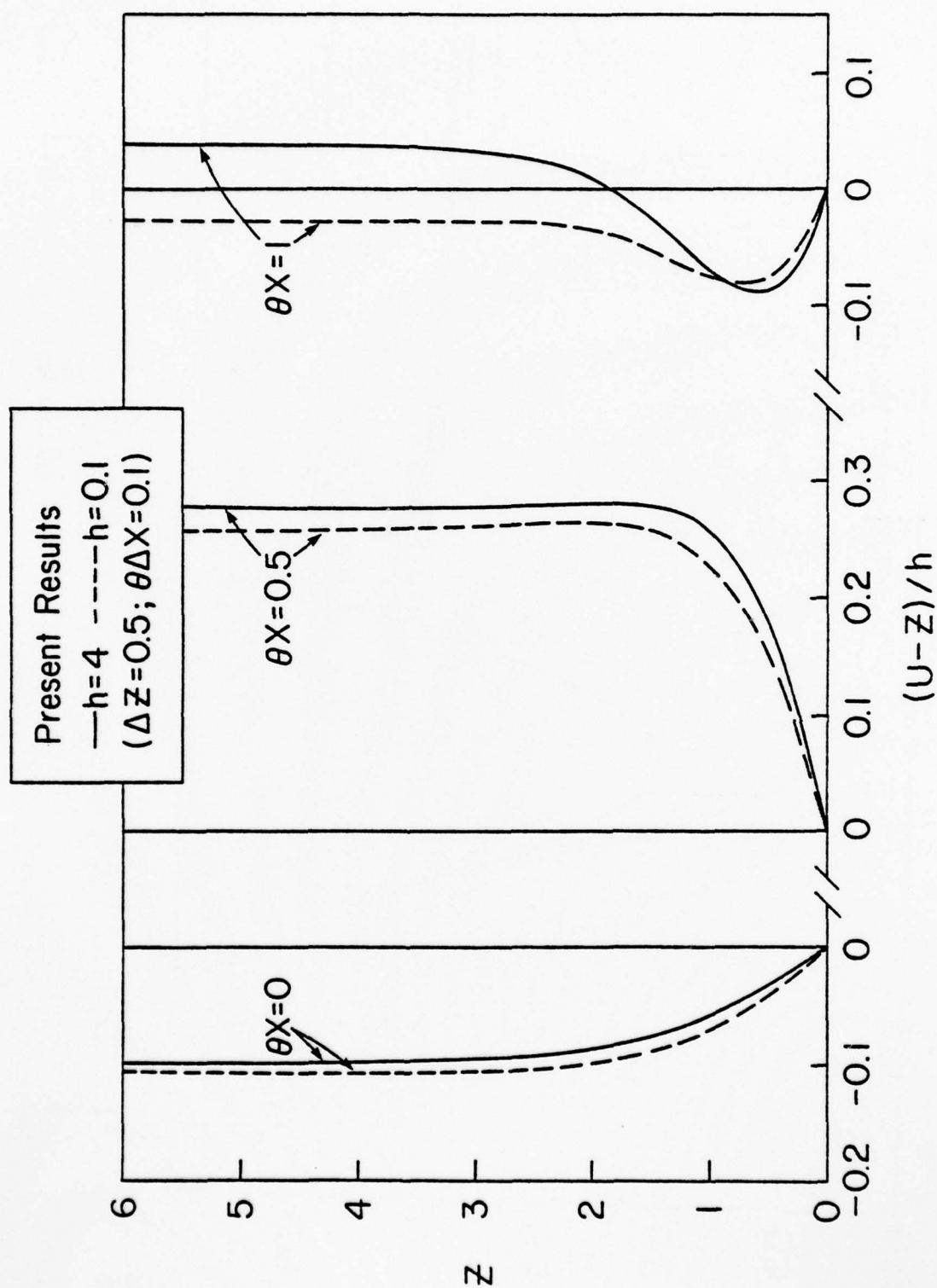


Fig. 8. Supersonic Flow Past a Parabolic Hump; Normalized Longitudinal Velocity Dependence on h .

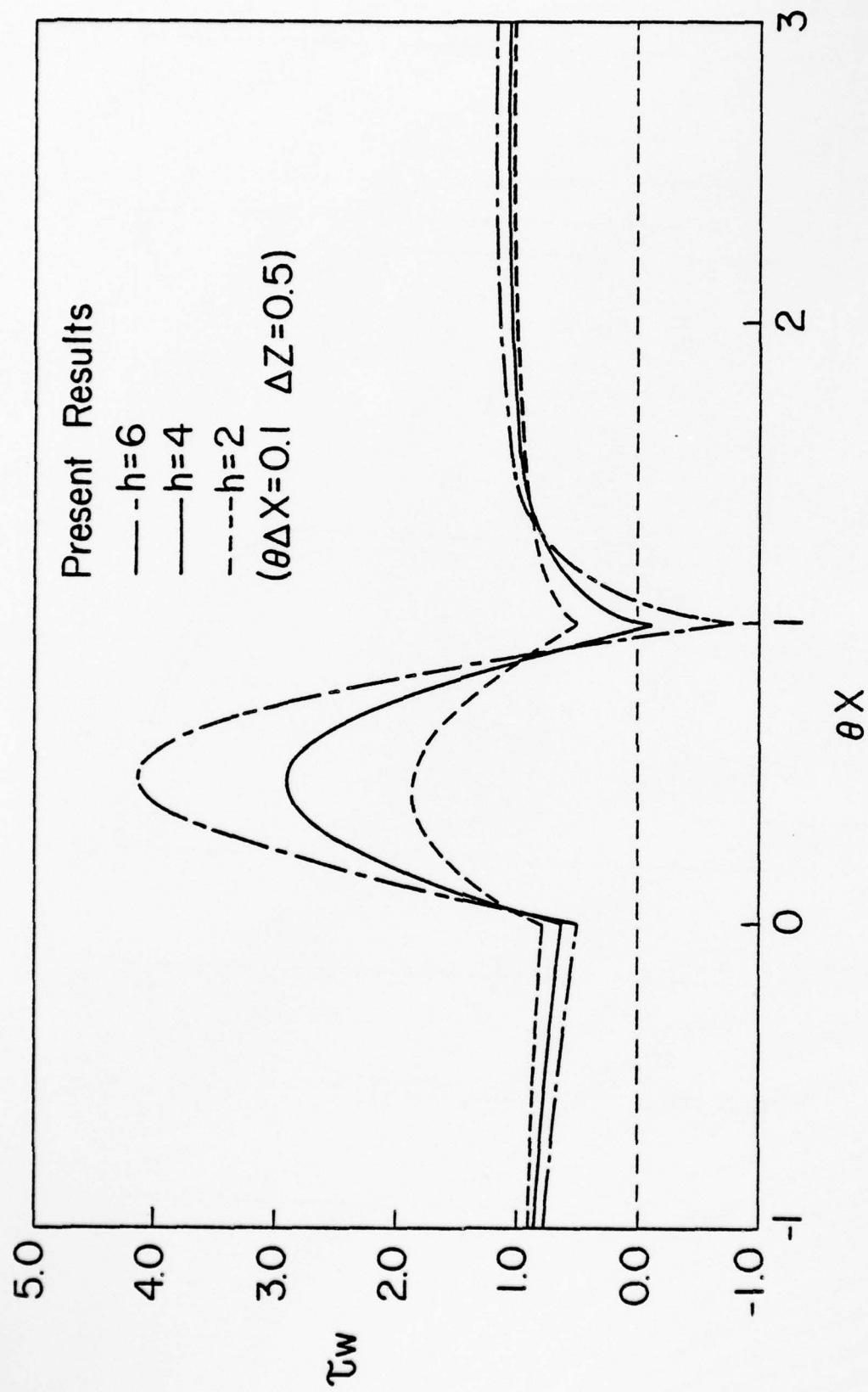


Fig. 9. Supersonic Flow Past a Parabolic Hump; Wall Shear Dependence on h .

AD-A060 203

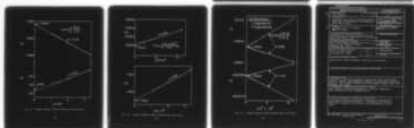
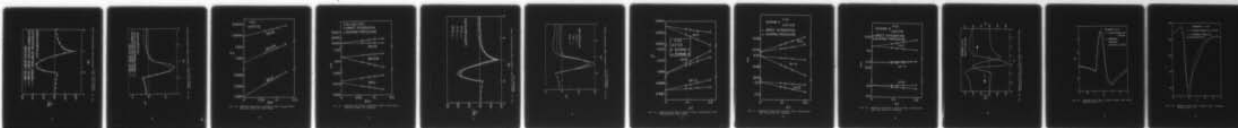
CINCINNATI UNIV OH DEPT OF AEROSPACE ENGINEERING AND--ETC F/G 20/4
NUMERICAL SOLUTIONS OF THE TRIPLE-DECK EQUATIONS FOR SUPERSONIC--ETC(U)
JUN 78 M NAPOLITANO, M J WERLE, R T DAVIS N00014-76-C-0359

UNCLASSIFIED

AFL-78-6-42

NL

2 OF 2
AD
AO 60203



END
DATE
FILMED
12-78

DDC

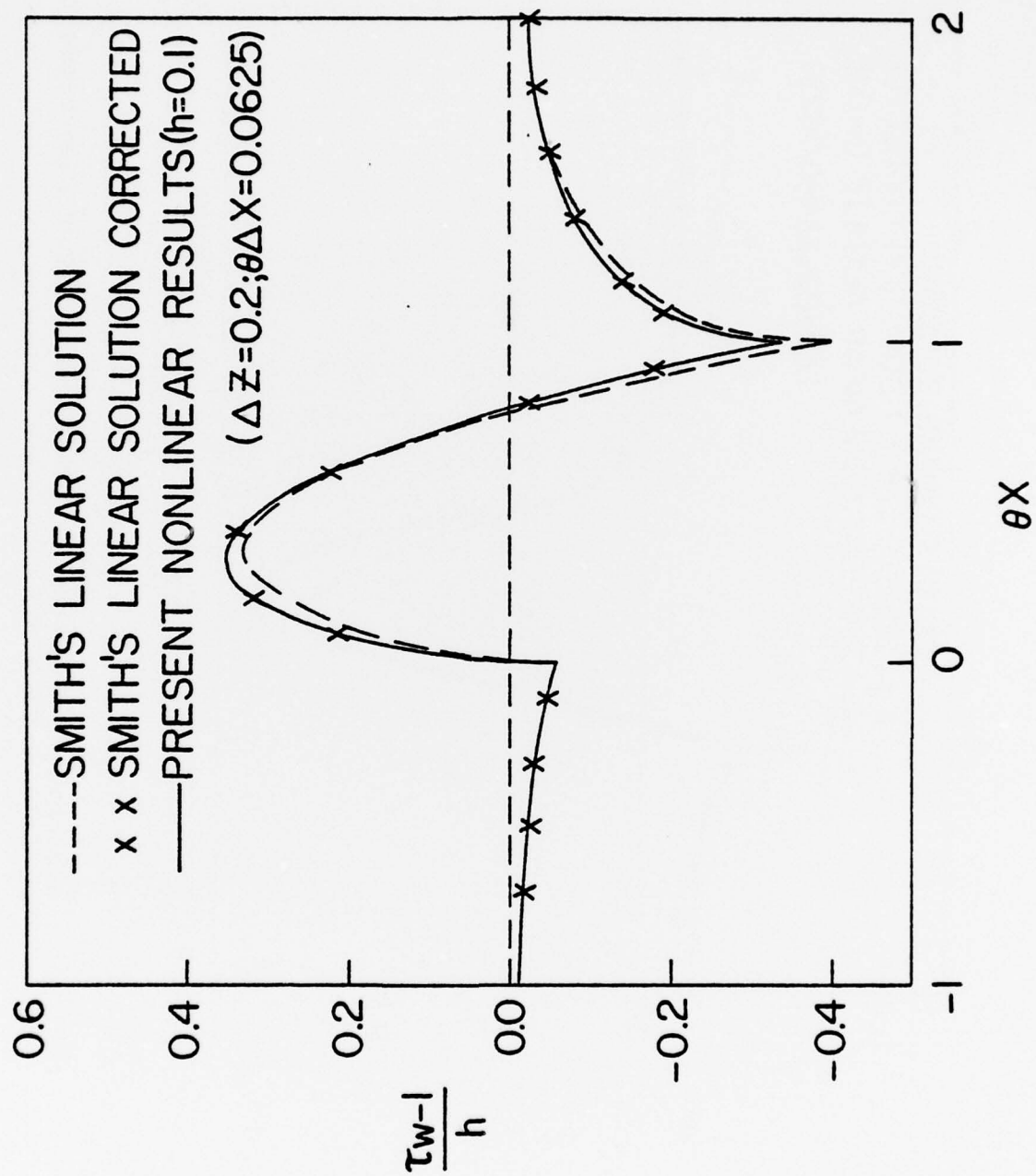


Fig. 10. Subsonic Flow Past a Parabolic Hump; Normalized Wall Shear Profile for $h = 0.1$.

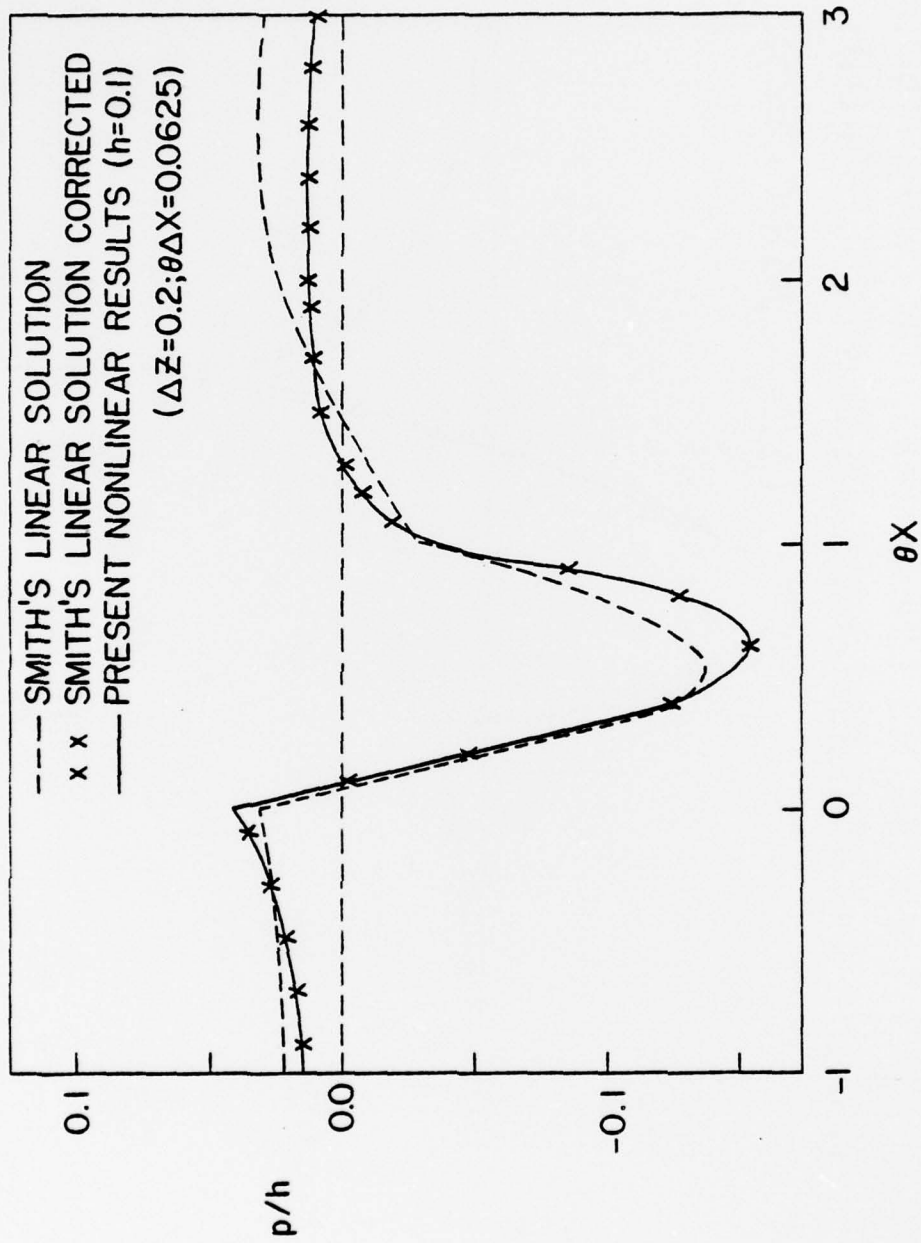


Fig. 11. Subsonic Flow Past a Parabolic Hump; Normalized Pressure Profile for $h = 0.1$.

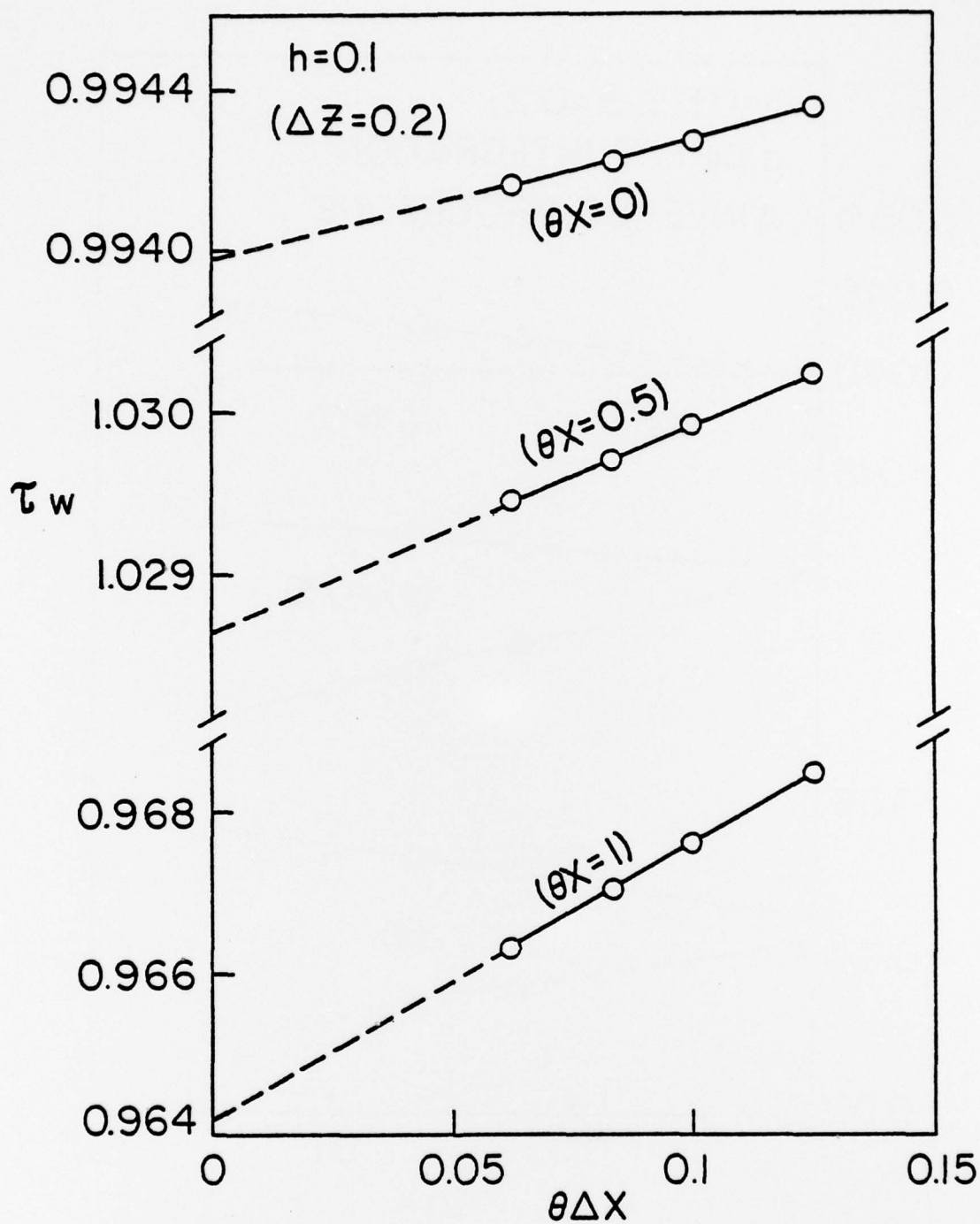


Fig. 12. Subsonic Flow Past a Parabolic Hump; Longitudinal Step Size Study for Wall Shear.

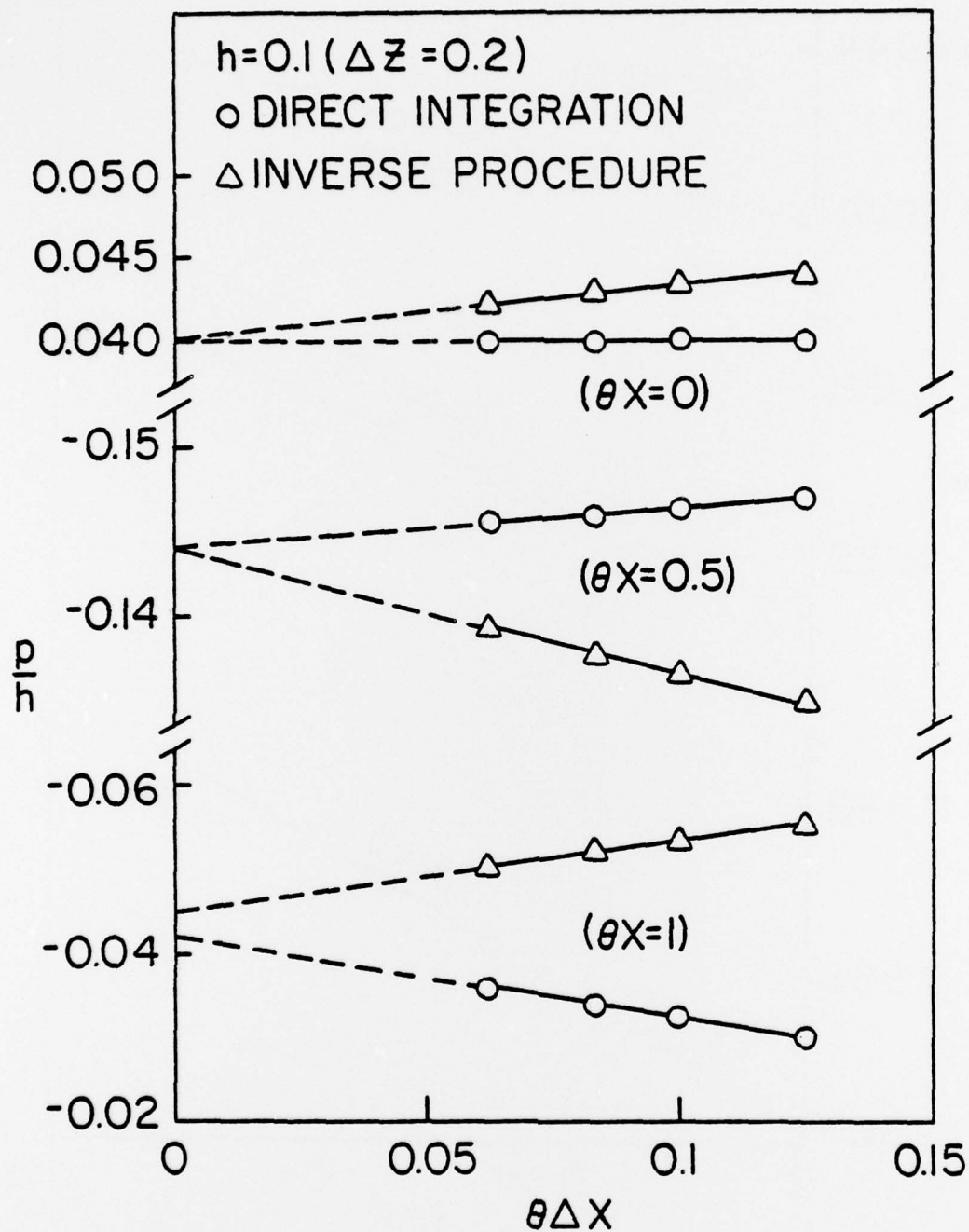


Fig. 13. Subsonic Flow Past a Parabolic Hump; Longitudinal Step Size Study for Pressure.

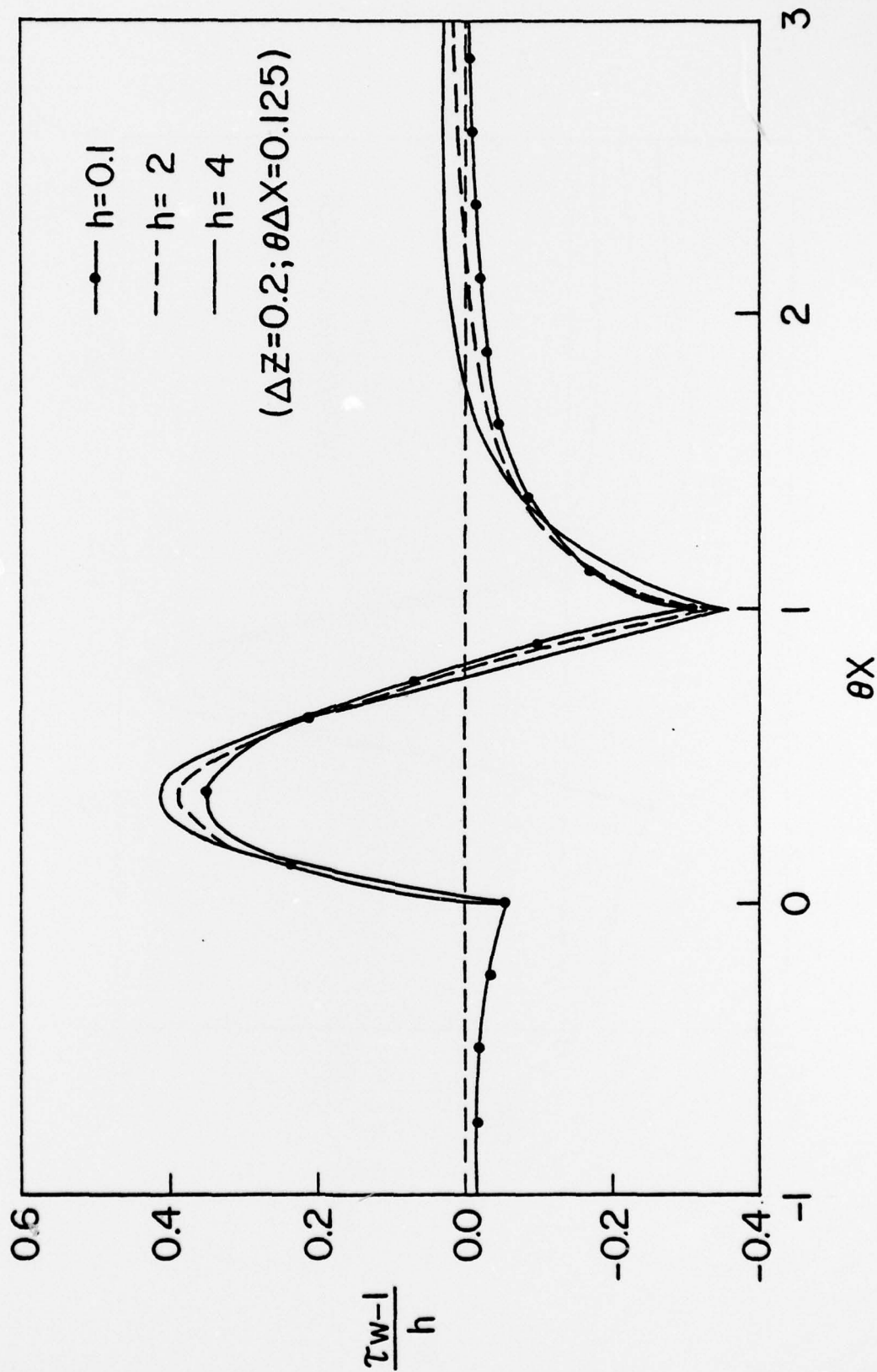


Fig. 14. Subsonic Flow Past a Parabolic Hump; Normalized Wall Shear Dependence on h .

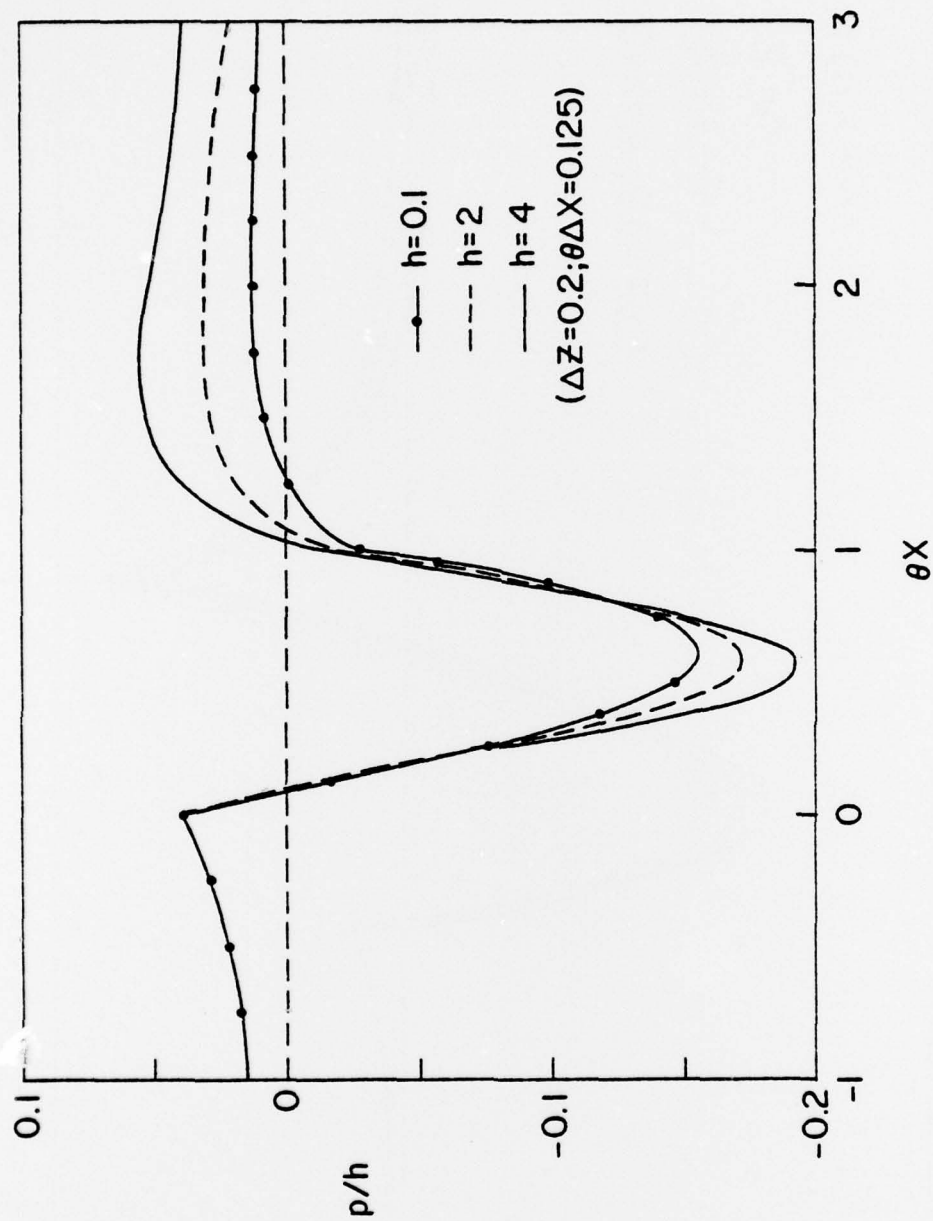


Fig. 15. Subsonic Flow Past a Parabolic Hump; Normalized Pressure Dependence on h .

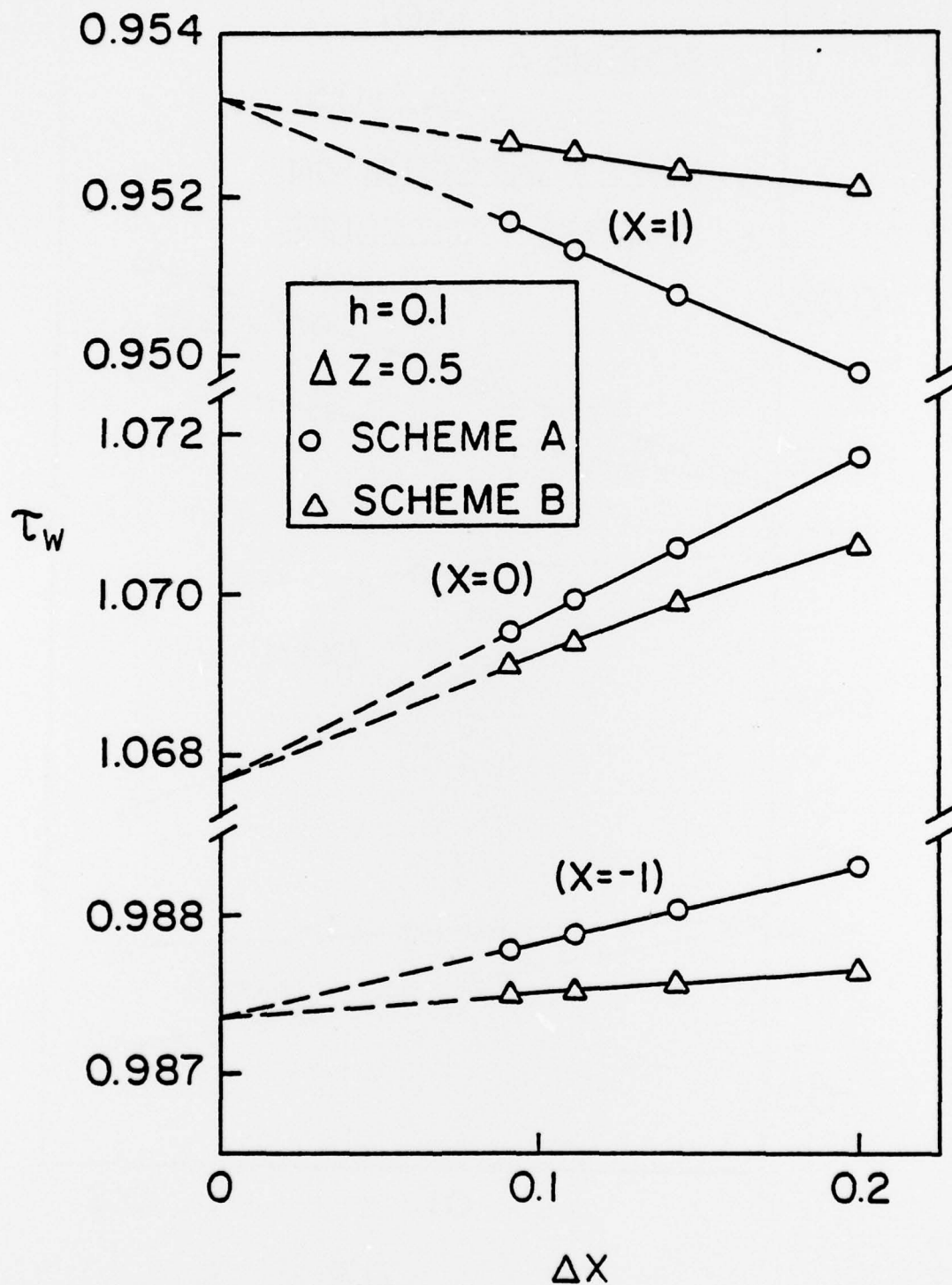


Fig. 16. Subsonic Flow Past a Quartic Hump; Longitudinal Step Size Study for Wall Shear.

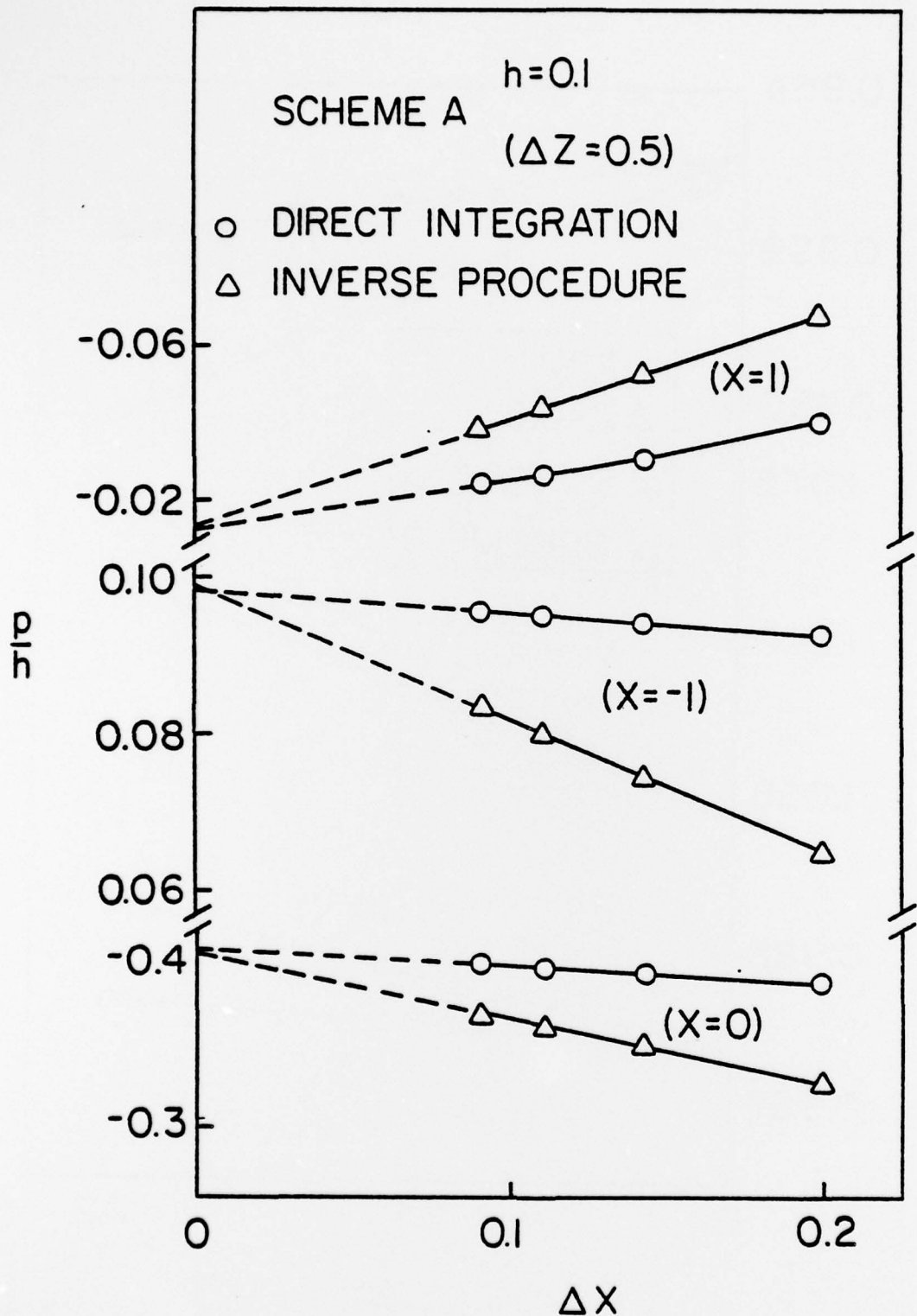


Fig. 17. Subsonic Flow Past a Quartic Hump; Longitudinal Step Size Study for Pressure.

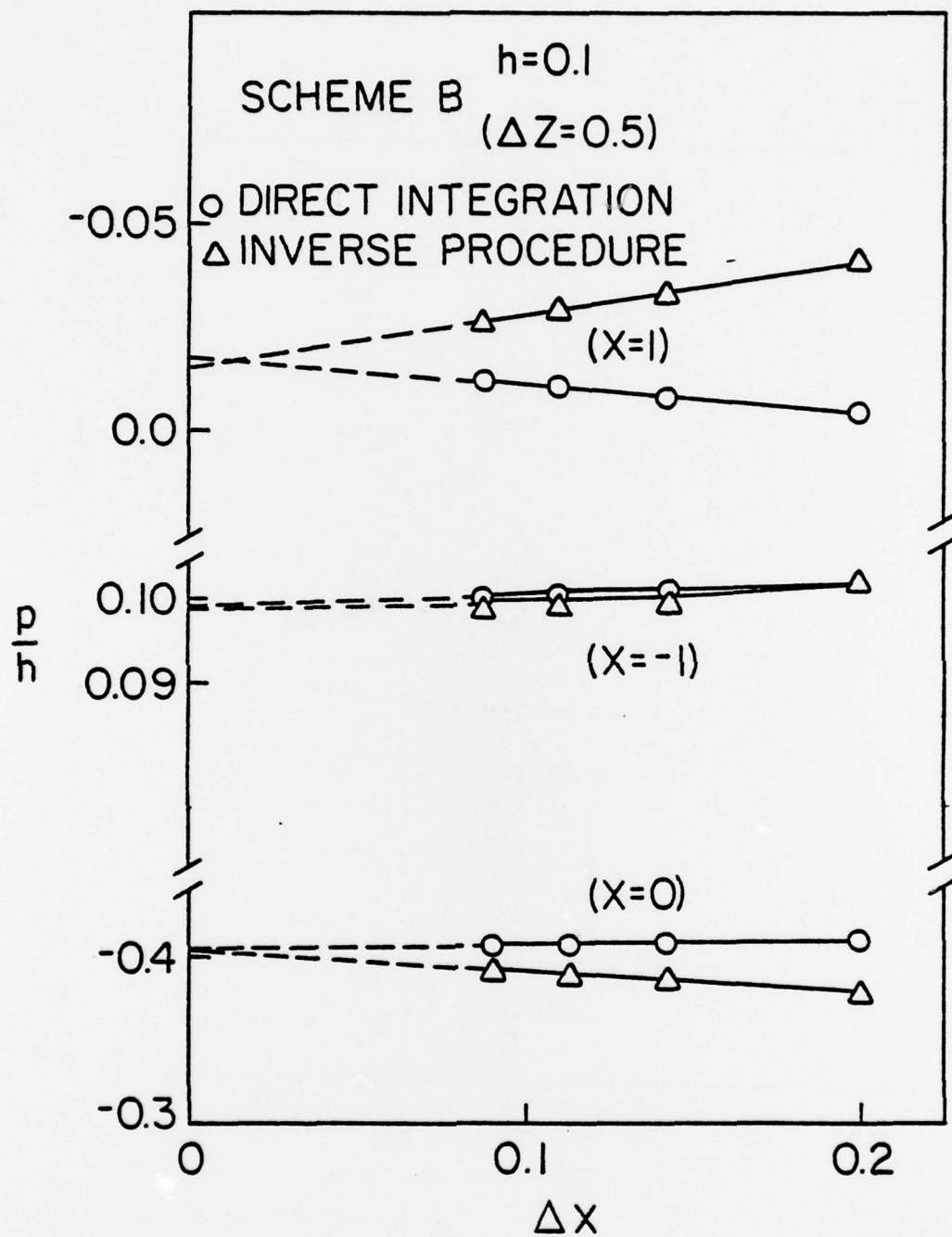


Fig. 18. Subsonic Flow Past a Quartic Hump; Longitudinal Step Size Study for Pressure.

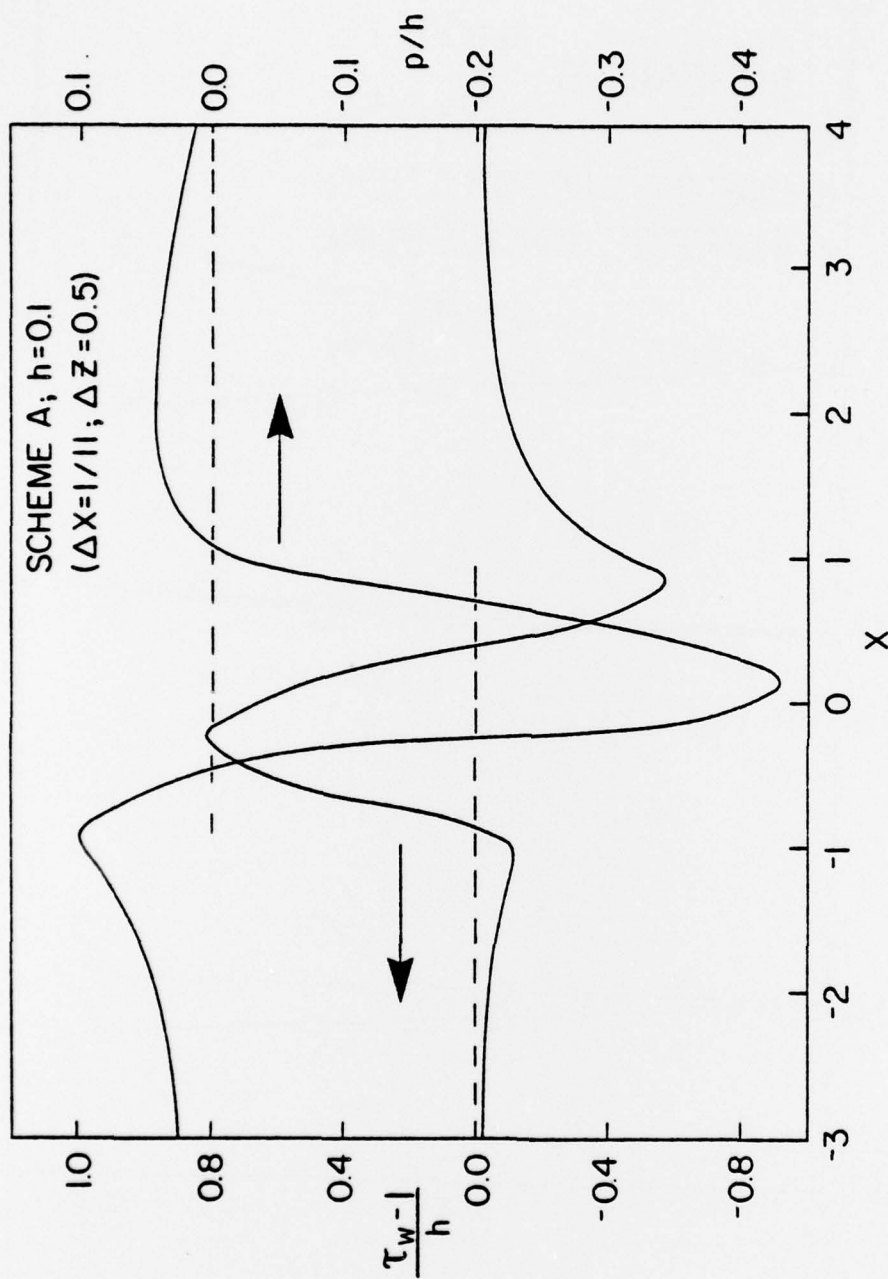


Fig. 19. Subsonic Flow Past a Quartic Hump; Normalized Wall Shear and Pressure Profiles for $h = 0.1$.

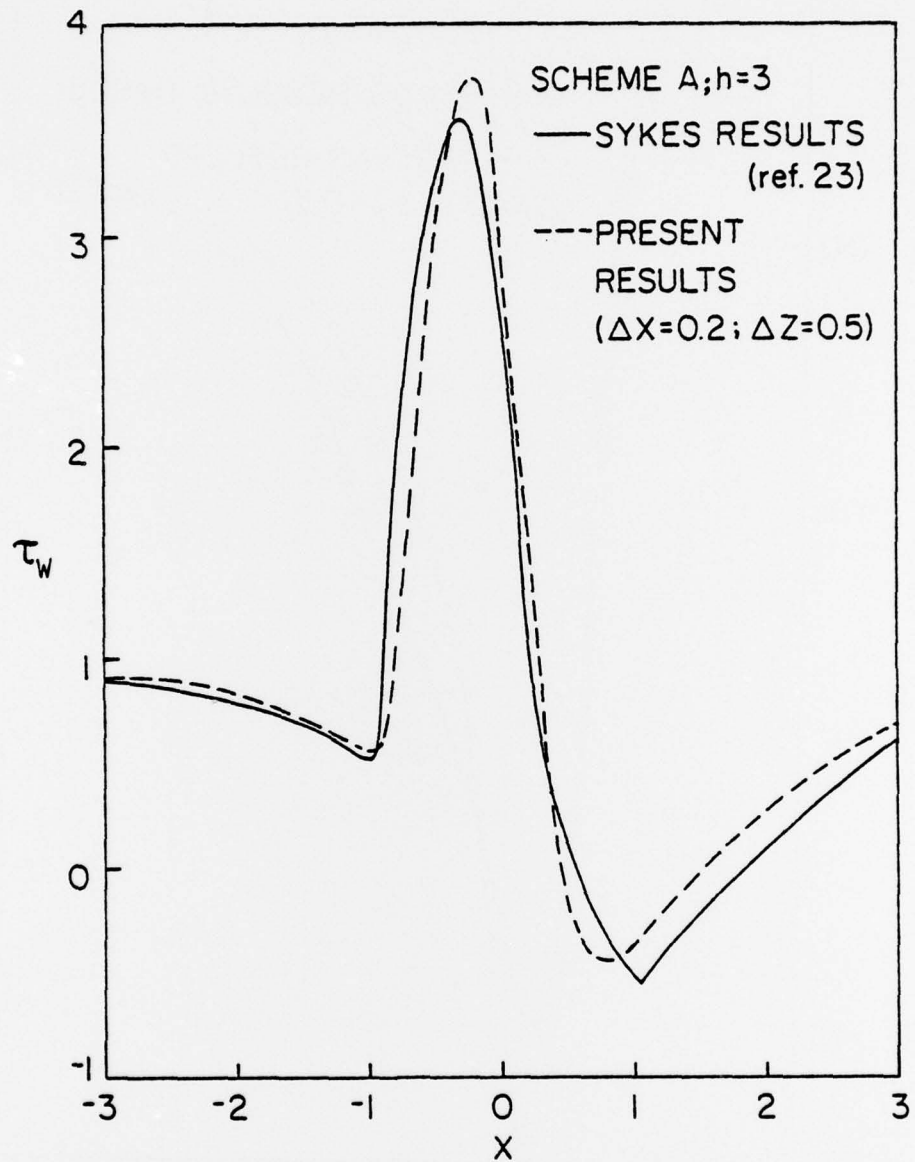


Fig. 20. Subsonic Flow Past a Quartic Hump; Wall Shear Profile for $h = 3$.

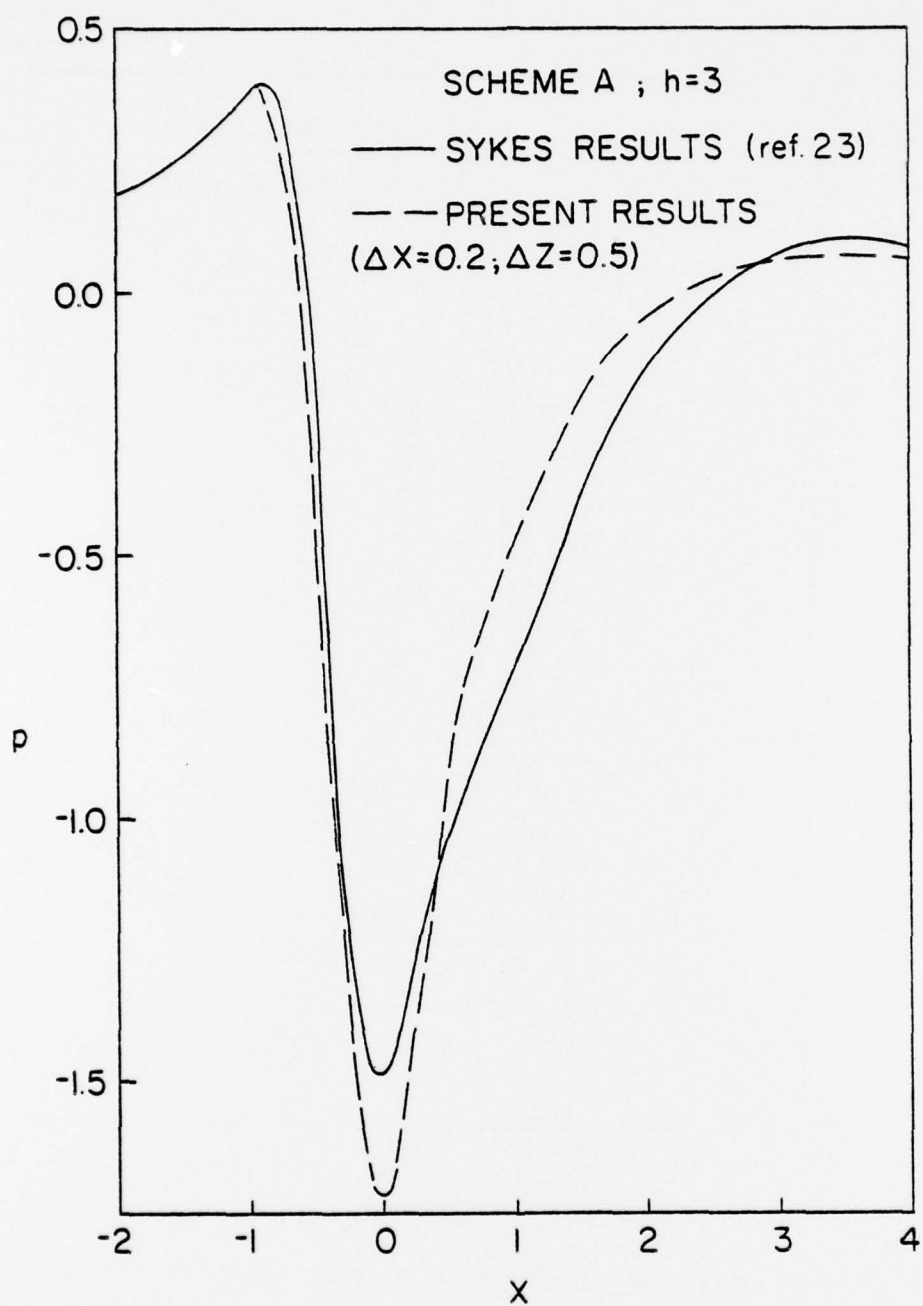


Fig. 21. Subsonic Flow Past a Quartic Hump; Pressure Profile for $h = 3$.

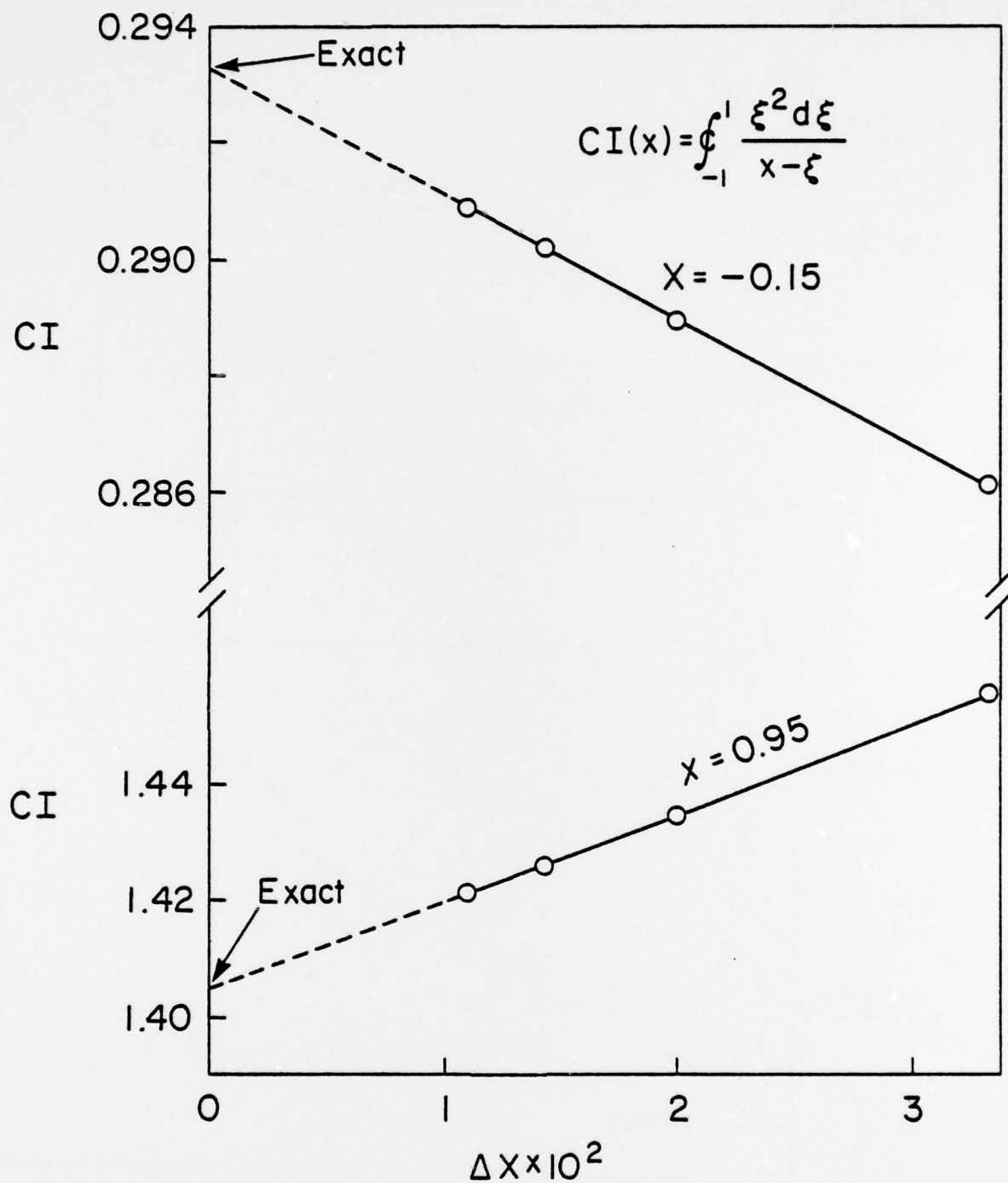


Fig. 22. Cauchy Integral Model Problem Step Size Study.

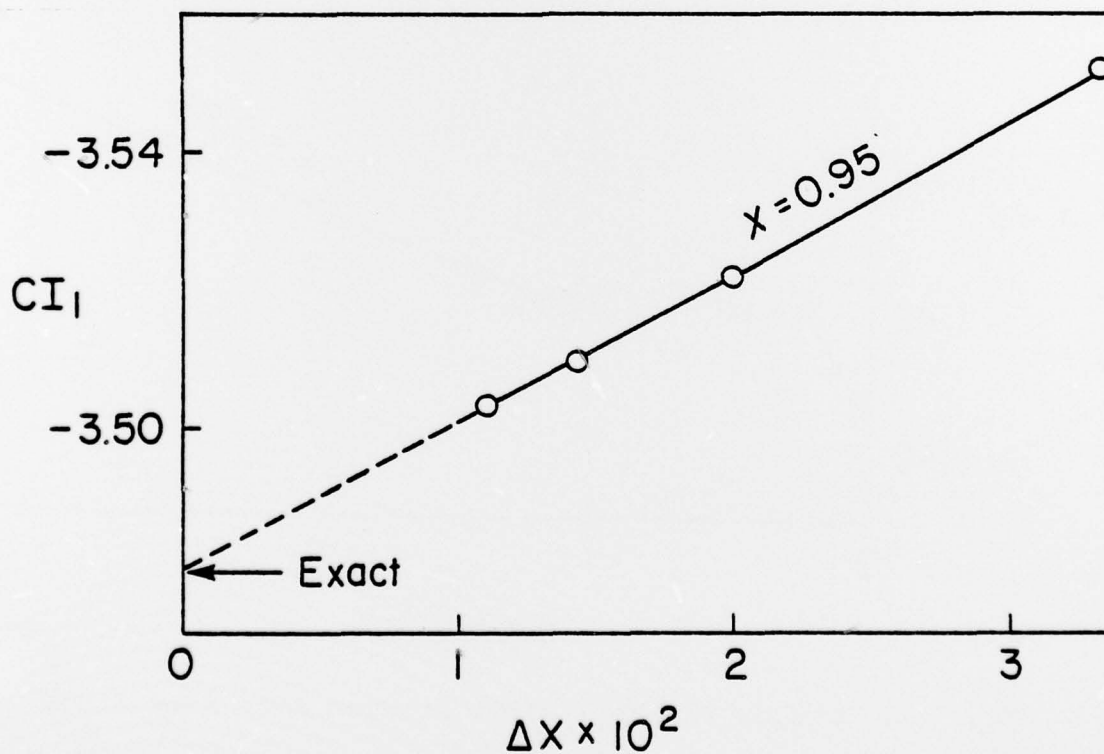
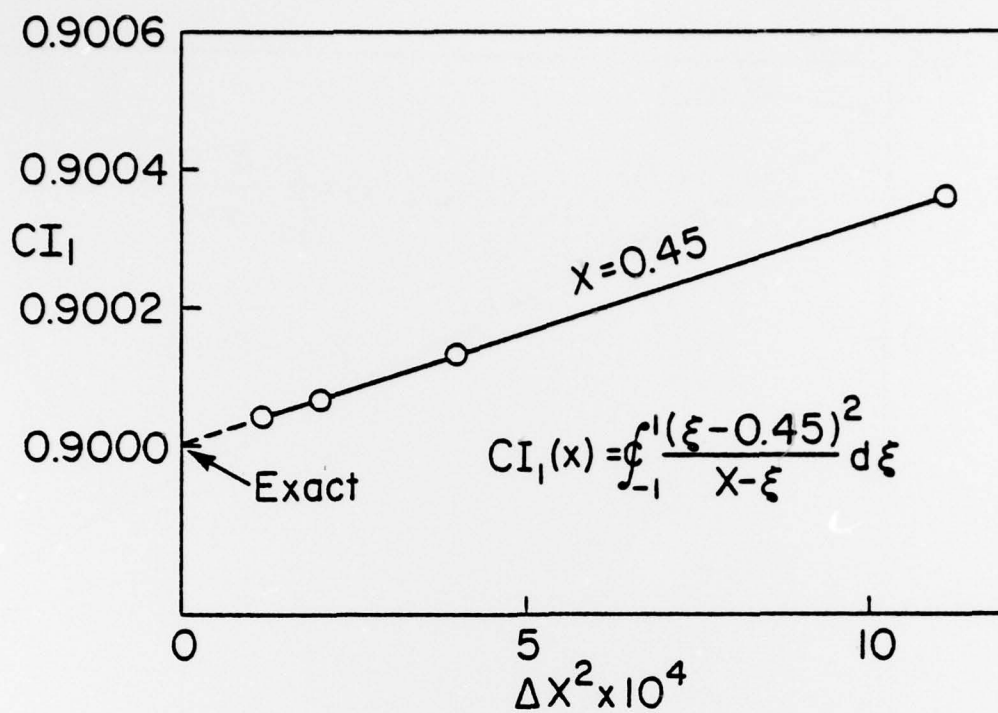


Fig. 23. Cauchy Integral Model Problem Step Size Study.

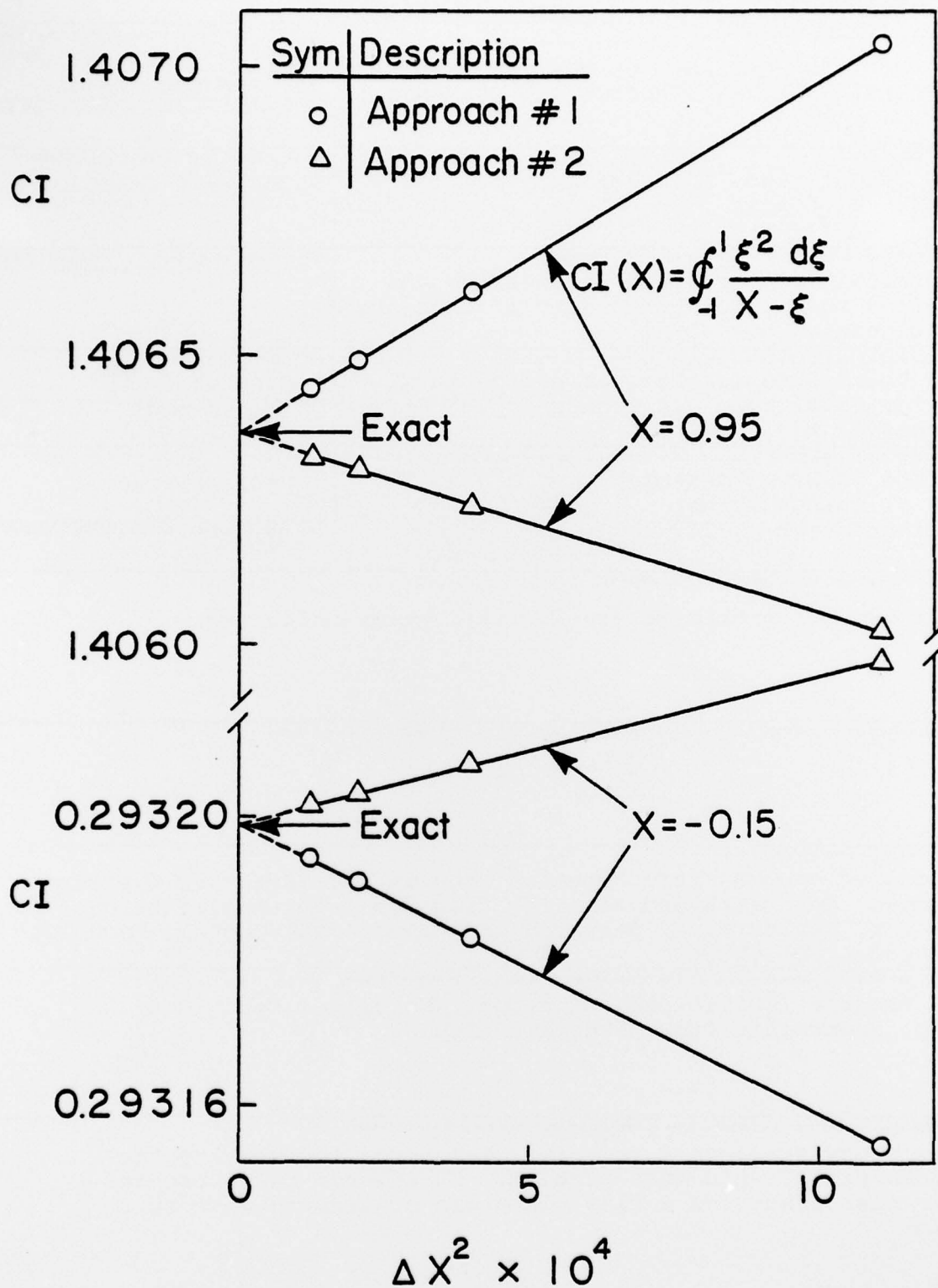


Fig. 24. Cauchy Integral Model Problem Step Size Study.

UNCLASSIFIED

SECURITY CLASSIFICATION OF THIS PAGE (When Data Entered)

REPORT DOCUMENTATION PAGE		READ INSTRUCTIONS BEFORE COMPLETING FORM
1. REPORT NUMBER AFL-78-6-42	2. GOVT ACCESSION NO.	3. RECIPIENT'S CATALOG NUMBER Rept
4. TITLE (and Subtitle) NUMERICAL SOLUTIONS OF THE TRIPLE-DECK EQUATIONS FOR SUPERSONIC AND SUBSONIC FLOW PAST A HUMP.		5. TYPE OF REPORT & PERIOD COVERED Final - 1 October 1976- 30 September 1978.
7. AUTHOR(s) M. Napolitano, M.J. Werle and R.T. Davis		6. PERFORMING ORG. REPORT NUMBER AFL 78-6-42
9. PERFORMING ORGANIZATION NAME AND ADDRESS Department of Aerospace Engineering and Applied Mechanics, University of Cincinnati Cincinnati, Ohio 45221		8. CONTRACT OR GRANT NUMBER(s) N00014-76-C-0359
11. CONTROLLING OFFICE NAME AND ADDRESS ONR Fluid Dynamics Program and David W. Taylor Naval Ship R&D Center Bethesda, MD 20084		10. PROGRAM ELEMENT, PROJECT, TASK AREA & WORK UNIT NUMBERS
14. MONITORING AGENCY NAME & ADDRESS (if different from Controlling Office) Office of Naval Research 800 N. Quincy Street Arlington, VA 22217		12. REPORT DATE June 1978
		13. NUMBER OF PAGES 101
		15. SECURITY CLASS. (of this report) Unclassified
		13a. DECLASSIFICATION/DOWNGRADING SCHEDULE
16. DISTRIBUTION STATEMENT (of this Report) Approved for public release; distribution unlimited.		
17. DISTRIBUTION STATEMENT (of the abstract entered in Block 20, if different from Report)		
18. SUPPLEMENTARY NOTES Sponsored by ONR Fluid Dynamics Program and Naval Sea Systems Command, General Hydromechanics Research Program Administered by David W. Taylor Naval Research and Development Center, Code 1505, Bethesda, MD 20084		
19. KEY WORDS (Continue on reverse side if necessary and identify by block number) GHR Program, Triple-Deck Equations, Numerical Technique, Hump, Supersonic Flow, Subsonic Flow.		
20. ABSTRACT (Continue on reverse side if necessary and identify by block number) This study presents a numerical technique for solving the fundamental Triple-Deck problem. Supersonic and subsonic flow past a hump on a flat plate are considered as a test case.		

DD FORM 1 JAN 73 1473

EDITION OF 1 NOV 63 IS OBSOLETE
S/N 0102-014-6601

UNCLASSIFIED

SECURITY CLASSIFICATION OF THIS PAGE (When Data Entered)

410677

15